

DYNAMICAL LOW-RANK APPROXIMATION STRATEGIES FOR NONLINEAR FEEDBACK CONTROL PROBLEMS

LUCA SALUZZI^{1,*} AND MARIA STRAZZULLO^{2,*}

ABSTRACT. This paper addresses the stabilization of dynamical systems in the infinite horizon optimal control setting using nonlinear feedback control based on State-Dependent Riccati Equations (SDREs). While effective, the practical implementation of such feedback strategies is often constrained by the high dimensionality of state spaces and the computational challenges associated with solving SDREs, particularly in parametric scenarios. To mitigate these limitations, we introduce the Dynamical Low-Rank Approximation (DLRA) methodology, which provides an efficient and accurate framework for addressing high-dimensional feedback control problems. DLRA dynamically constructs a compact, low-dimensional representation that evolves with the problem, enabling the simultaneous resolution of multiple parametric instances in real-time.

We propose two novel algorithms to enhance numerical performances: the cascade-Newton-Kleinman method and Riccati-based DLRA (R-DLRA). The cascade-Newton-Kleinman method accelerates convergence by leveraging Riccati solutions from the nearby parameter or time instance, supported by a theoretical sensitivity analysis. R-DLRA integrates Riccati information into the DLRA basis construction to improve the quality of the solution. These approaches are validated through nonlinear one-dimensional and two-dimensional test cases showing transport-like behavior, demonstrating that R-DLRA outperforms standard DLRA and Proper Orthogonal Decomposition-based model order reduction in both speed and accuracy, offering a superior alternative to Full Order Model solutions.

1. INTRODUCTION

Optimal control of dynamical systems is a central topic in diverse scientific fields. Indeed, it is ubiquitous in many engineering and industrial applications based on the stabilization of nonlinear dynamical systems toward a dynamic equilibrium. Nonlinear stabilization is commonly addressed through the implementation of feedback (closed-loop) controllers. Unlike open-loop controls, these controllers provide superior stability features in the presence of external disturbances. The design of optimal feedback controls typically relies on dynamic programming, which formulates the optimal feedback policy as the solution to a Hamilton-Jacobi-Bellman (HJB) nonlinear Partial Differential Equation (PDE). The progress in the solution of HJB PDEs for optimal control is significant. For example, substantial attention has been drawn to sparse grids strategies [15], tree-structure approaches [13], applications of artificial neural networks [7, 27, 40] and regression-type methods in tensor formats [29, 10].

In this study, we address the problem of feedback stabilization by employing an alternative methodology that integrates concepts from dynamic programming and nonlinear model predictive control. Specifically, we utilize the State-Dependent Riccati Equation (SDRE) approach [6]. Unlike traditional methods that require solving the HJB equation, which is often computationally prohibitive for nonlinear systems, the SDRE approach offers a practical and computationally efficient alternative. By reformulating the control problem into a state-dependent framework, the SDRE method enables the synthesis of near-optimal feedback controllers while avoiding the numerical burden associated with the direct solution of the HJB equation.

¹ DIPARTIMENTO DI MATEMATICA, SAPIENZA UNIVERSITÀ DI ROMA, PIAZZALE ALDO MORO, 5, ROMA, 00185, ITALY.

² POLITECNICO DI TORINO, DEPARTMENT OF MATHEMATICAL SCIENCES “GIUSEPPE LUIGI LAGRANGE”, CORSO DUCA DEGLI ABRUZZI, 24, 10129, TORINO, ITALY.

* INDAM, GNCS MEMBER.

E-mail address: luca.saluzzi@uniroma1.it, maria.strazzullo@polito.it.

Date: January 14, 2025.

The SDRE approach operates by solving a sequence of algebraic Riccati equations along a trajectory in the state space. For high-dimensional Riccati equations, effective *ad hoc* solvers are available, such as those described in [22, 4]. In this contribution, we employ the Newton-Kleinman (NK) strategy, an iterative technique that solves the linearized Riccati equation at each step until a specified convergence criterion is achieved [23]. Despite the availability of advanced iterative solvers, the application of the SDRE approach remains challenging, particularly in the context of time-dependent parametric settings. These scenarios require solving numerous high-dimensional Riccati equations across a wide range of parameters and time instances, posing significant computational demands for control design and implementation. Nevertheless, nonlinear control theory can be of utmost importance in real-time and many query contests, despite the limited applicability due to the burden of the computational costs. For this reason, Reduced Order Models (ROMs) for control problems have recently gained increasing attention in the scientific community. ROMs build a low-dimensional framework spanned by basis functions related to properly chosen parametric instances in an *offline stage*. Once provided the reduced space, a novel evaluation of the parameter is performed by a Galerkin projection in an *online phase*. In this way, ROMs are faster than the Full Order Model (FOM) upon which they are built, and solve the system with a certain degree of accuracy. Here, we report a non-exhaustive list of contributions to the field based on linear projection-based ROM for nonlinear control in open-loop [17, 25, 32, 38, 39] and closed-loop contexts [26, 18, 1, 21, 8]. The presented strategies can provide a robust and efficient representation, however, they might fail in transport and wave-like settings, where a large number of basis functions is needed to achieve an acceptable accuracy [9]. Many strategies have been proposed to overcome this issue, the interested reader may refer to the complete literature overview proposed in [31] and the reference therein.

In this work, we deal with parametric nonlinear infinite horizon optimal control problems, using a nonlinear projection-based ROM whose basis functions evolve over time and follow the system dynamics. We exploit the Dynamical Low-Rank Approximation (DLRA) [24], introduced to efficiently compute approximations of large-scale time-dependent problems exploiting time integration in the tangent space of the reduced representation of the solution. DLRA provides a compact representation of the system and the evolution of the basis ensures an increased accuracy if compared to standard data-compression techniques such as Proper Orthogonal Decomposition (POD), see, e.g., [34] for stochastic PDEs and [30] for Hamiltonian systems. The application of the DLRA methodology in the context of optimal control and the HJB equation was previously explored in [12], where the authors addressed the approximation of finite horizon optimal control problems. Their approach leverages policy iteration and a dynamical low-rank approximation in tensor format for the value function.

In contrast, this work focuses on an infinite horizon parametric setting, solved using the SDRE technique. Here, the DLRA is employed to achieve a compact and efficient representation of the solution to the parametric dynamical system.

Moreover, we propose novel strategies to (i) accelerate the solution of SDREs arising from time integration and (ii) enhance the accuracy of DLRA by incorporating information on the control action and the SDRE solution. This leads to the development of a Riccati-based DLRA (R-DLRA), which adapts concepts from [35, 36] to further refine the methodology.

The originality of this contribution relies on:

- a novel strategy to solve iteratively the SDRE guided by a theoretical sensitivity analysis: the cascade-Newton-Kleinman (C-NK) method. The C-NK exploits the parametric and evolutive information of the system to accelerate the convergence of the classical NK, providing a faster tool to solve Riccati problems both at the FOM and ROM level;
- the application of the DLRA approach combined to C-NK for infinite horizon optimal control problems solved by SDRE. The DLRA proves to be a fast and efficient method for representing controlled dynamics in scenarios that pose significant challenges for traditional linear projection-based ROMs;
- the enhancement of the classical DLRA approach employing the Riccati information denoted as R-DLRA. The basis functions of the DLRA are enriched with basis functions related to

the SDRE or the control action. These additional basis functions increase the accuracy of the DLRA and serve as a tailored strategy for control problems.

The DLRA and R-DLRA algorithms provide a fascinating alternative to POD to address the *curse of dimensionality* of control applications under transport phenomena. We validate our findings with one-dimensional and two-dimensional nonlinear test cases.

The paper is outlined as follows: in Section 2, we introduce the parametric infinite horizon feedback control problem we address, the SDRE deriving from the control system, its numerical approximation, and the novel C-NK approach. Section 3 provides a theoretical justification for the employment of the C-NK. Section 4 introduces DLRA and its extension to feedback control. In Section 5 we propose two novel R-DLRA strategies based on the enhancement of DLRA with Riccati information and C-NK approach. The numerical algorithms are validated in Section 6, where we compare the performance of DLRA, R-DLRA, and POD in terms of computational efficiency and accuracy against the FOM solution for feedback control problems based on the Burgers' equation in one and two dimensions. Conclusions follow in Section 7.

2. PROBLEM FORMULATION

This section introduces the parametric infinite horizon nonlinear feedback control problem we deal with in this contribution. The problem formulation is described in Section 2.1, while the SDRE method is described in Section 2.2. Finally, in Section 2.3, we discuss the numerical approximation of SDREs.

2.1. Parametric infinite horizon feedback control. We now focus on asymptotic stabilization by infinite horizon optimal control in a parametric setting. Given a parameter $\mu \in \mathcal{P} \subset \mathbb{R}^n$, with $n \in \mathbb{N}$, the main objective is to minimize the following *cost functional*

$$(2.1) \quad \min_{u(\cdot) \in \mathcal{U}_{ad}} J(u(\cdot), y_0; \mu) = \int_0^\infty y(s; \mu)^\top Q y(s; \mu) + u(s; \mu)^\top R u(s; \mu) ds,$$

subject to a nonlinear dynamics

$$(2.2) \quad \dot{y}(t; \mu) = f(y(t; \mu)) + Bu(t; \mu), \quad y(0; \mu) = y_0(\mu),$$

where $y(t; \mu)$ is the *state* variable represented by a column vector in \mathbb{R}^{N_h} , $u(\cdot; \mu) \in \mathcal{U}_{ad} = \{u : \mathbb{R}^+ \rightarrow U \subset \mathbb{R}^m, \text{ measurable}\}$ is the *control* variable, $f : \mathbb{R}^{N_h} \rightarrow \mathbb{R}^{N_h}$ is the system dynamics, $B \in \mathbb{R}^{N_h \times m}$ is the control matrix, $Q \in \mathbb{R}^{N_h \times N_h}$ is a symmetric semidefinite matrix, $R \in \mathbb{R}^{m \times m}$ is a symmetric positive definite matrix, and $y_0(\mu)$ is a parametric initial condition.

For the sake of notation, we write the state and the control in a more compact form as $y_{\mu,t} = y(t; \mu)$ and $u_{\mu,t} = u(t; \mu)$. Following the same notation, the parametric initial condition will be $y_0(\mu) = y_{\mu,0}$. We will use both the extended and the compact notations, depending on the needs.

One method for the resolution of the optimal control problem (2.1)-(2.2) involves solving the HJB equation, a first-order nonlinear PDE defined in \mathbb{R}^{N_h} .

In many applications, the dimension N_h may be large and yields the *curse of dimensionality*, a phenomenon where the computational resources required to solve the HJB grow exponentially with N_h . This is a significant limitation of traditional numerical methods. Standard grid-based approaches, for instance, become computationally infeasible as the required number of grid points increases exponentially in higher dimensions. In contrast to these computationally intensive approaches, a widely used alternative in practical applications is the SDRE method, which balances computational efficiency and control performance in high-dimensional settings.

2.2. State-Dependent Riccati Equation. The SDRE is a powerful mathematical tool with broad-ranging practical uses [6]. As a natural extension of the traditional Riccati equation, the SDRE expands its versatility by integrating state-dependent coefficients, thereby adapting to nonlinear and fluctuating systems. This method hinges on sequentially solving linear-quadratic control

tasks derived from a step-by-step linearization of the dynamics. In this work, we will always suppose that the dynamical system (2.2) is expressed in semilinear form, i.e.:

$$\begin{aligned} \dot{y}(t; \mu) &= A(y(t; \mu))y(t; \mu) + Bu(t; \mu), \\ y(0, \mu) &= y_{\mu,0}. \end{aligned}$$

Assuming that the system dynamics are linear with respect to the state, i.e., $A(y(t)) = A \in \mathbb{R}^{N_h \times N_h}$, the problem reduces to what is commonly known as the Linear Quadratic Regulator (LQR) problem. In this context, we introduce the notions of stabilizability and detectability, which will play a crucial role in the subsequent analysis.

Definition 2.1. *The pair (A, B) is stabilizable if there exists a feedback matrix $K \in \mathbb{R}^{n \times m}$ such that $A - BK$ is stable, i.e., if all its eigenvalues lie on the open left half complex plane.*

Definition 2.2. *The pair (A, C) is detectable if the pair (A^\top, C^\top) is stabilizable.*

We suppose that the pair (A, B) is stabilizable and the pair $(A, Q^{1/2})$ is detectable. In this case, for a given state y , the feedback control is determined by the following relation

$$(2.3) \quad u(y) = -R^{-1}B^\top Py,$$

where $P \in \mathbb{R}^{N_h \times N_h}$ is the unique positive semidefinite solution of the Algebraic Riccati Equation (ARE)

$$A^\top P + PA - PBR^{-1}B^\top P + Q = 0.$$

For the sake of notation, let $F = BR^{-1}B^\top$. In essence, the SDRE technique extends this approach by incorporating a state-dependence in the Riccati solution, leading to the following feedback law:

$$(2.4) \quad u(y) = -R^{-1}B^\top P(y)y,$$

where $P(y)$ now serves as the solution to a SDRE defined as

$$(2.5) \quad A^\top(y)P(y) + P(y)A(y) - P(y)FP(y) + Q = 0,$$

with $A(y)$ fixed at the state y . In general, this iterative process can be applied along the parametric trajectory, sequentially solving (2.5) as the state $y_{\mu,t}$ evolves. The controlled dynamics now reads

$$(2.6) \quad \begin{cases} \dot{y}(t; \mu) &= A_{cl}(y(t; \mu))y(t; \mu), \\ y_{\mu,0} &= x(\mu), \end{cases}$$

where $A_{cl}(y(t; \mu)) = A(y(t; \mu)) - FP(y(t; \mu))$ is called closed-loop matrix. We assume that the stabilizability and detectability conditions are satisfied for all states y within a domain Ω .

Assumption 2.3. *The pair $(A(x), B)$ and $(A(x), Q^{1/2})$ are pointwise stabilizable and detectable, respectively, for every $x \in \Omega$.*

Under these conditions, the SDRE (2.5) is guaranteed to have a unique positive semidefinite solution for all $y \in \Omega$ (see, e.g., [28]). Under the additional assumption that $f \in C^1(\mathbb{R}^{N_h})$, it can be shown that the controlled dynamics arising from the system in (2.6) converges locally to the target state (for precise statements and further elaboration, see [2]).

We now emphasize the dependence of the Riccati solution on the parameter μ and time t , denoting it as $P_{\mu,t} = P(y(t; \mu))$. This distinction is crucial for the findings in this contribution, particularly for the tailored approaches to solve parametric nonlinear feedback control problems by employing SDREs. In what follows, we describe the numerical solver we used to deal with the solution of (2.5).

2.3. Numerical approximation of the SDRE. Motivated by the parametric and time-dependent nature of our setting, which results in a repeated high computational effort, we propose to solve the SDRE in (2.5) using an iterative method instead of a direct one. Specifically, we pay peculiar attention to the choice of the *initial guess* of the nonlinear solver. Indeed, the Riccati solution approximated at a given time instance and parameter value can serve as an effective initial guess for approximating the Riccati solution at a different time or parameter value. This methodology will be further clarified in Section 3, where we establish conditions under which such initialization enhances the effectiveness of the iterative scheme. First of all, let us define the *residual* of the SDRE as

$$(2.7) \quad \mathcal{R}_{(\mu,t)}(P_{\mu,t}) = A_{\mu,t}^\top P_{\mu,t} + P_{\mu,t} A_{\mu,t} - P_{\mu,t} F P_{\mu,t} + Q,$$

with $A_{\mu,t} = A(y_{\mu,t})$. In other words, given a pair $(\mu, t) \in \mathcal{P} \times \mathbb{R}^+$, solving the SDRE translates into finding the solution to $\mathcal{R}_{(\mu,t)}(P_{\mu,t}) = 0$. Due to the nonlinear nature of (2.7), a Newton method can be applied to reach an approximation of the solution. In particular, given an initial guess $P_{\mu,t}^0$, at the $(k+1)$ -th iteration of the method we solve

$$(2.8) \quad \mathcal{R}'_{(\mu,t)}[P_{\mu,t}^k](\delta P_{\mu,t}) = -\mathcal{R}_{(\mu,t)}(P_{\mu,t}^k) \quad \text{with the update} \quad P_{\mu,t}^{k+1} = P_{\mu,t}^k + \delta P_{\mu,t},$$

where $\mathcal{R}'_{(\mu,t)}[P_{\mu,t}^k]$ denotes the Fréchet derivative of the residual. Specifically, at each iteration, given the previous iterate $P_{\mu,t}^k$, we solve the Lyapunov equation

$$(2.9) \quad A_{cl}^k(y_{\mu,t})^\top P_{\mu,t}^{k+1} + P_{\mu,t}^{k+1} A_{cl}^k(y_{\mu,t}) = -P_{\mu,t}^k F P_{\mu,t}^k - Q,$$

with $A_{cl}^k(y_{\mu,t}) = A_{\mu,t} - F P_{\mu,t}^k$, generating a sequence $\{P_{\mu,t}^k\}_{k \geq 0}$. Under suitable assumptions, it is possible to prove that the sequence $\{P_{\mu,t}^k\}_{k \geq 0}$ converges to the unique solution of the SDRE (see, e.g., [23]).

Theorem 2.4. *Let $P_{\mu,t}^0 \in \mathbb{R}^{N_h \times N_h}$ be symmetric and positive semidefinite and such that $A_{\mu,t} - F P_{\mu,t}^0$ is stable, and let Assumption 2.3 hold. Then the Newton iterates $\{P_{\mu,t}^k\}_k$ converges to the unique solution of the SDRE.*

This strategy, denoted as Newton-Kleinman (NK) [23], is summarized in Algorithm 1. We remark that the Lyapunov equation is solved via the Matlab function `lyap`, based on the Bartels-Stewart's strategy [3].

Algorithm 1 The NK algorithm

Input: $A(\cdot)$, F , Q , tolerance `tol`, initial guess $P_{\mu,t}^0$
Output: solution of the SDRE, i.e., $P_{\mu,t}$

- 1: $k = 0$
 - 2: **while** $\|\mathcal{R}_{\mu,t}(P_{\mu,t}^k)\| \geq \text{tol}$ **do**
 - 3: Given $P_{\mu,t}^k$, solve (2.9) to get $P_{\mu,t}^{k+1}$
 - 4: $k = k + 1$
 - 5: **end while**
-

As in any Newton-based method, the initial guess plays a fundamental role in the NK strategy. Indeed, a proper choice for $P_{\mu,t}^0$ in the NK algorithm can significantly accelerate the convergence towards the unique positive semidefinite solution of the SDRE. In this work, we propose a *parameter-based selection of the guess*. That is, for two different parameters μ_i and μ_{i+1} with $\mu_i < \mu_{i+1}$, we solve the SDRE for $P_{\mu_{i+1},t}$ by leveraging the information from $P_{\mu_i,t}$ for a given t . Following the ideas behind *continuation* methods [19], we propose using $P_{\mu_i,t}$ as the initial guess for solving the SDRE for $P_{\mu_{i+1},t}$, thereby ensuring faster convergence of the NK towards the next parametric solution of the SDRE. Moreover, in Section 3, we demonstrate that, under suitable assumptions, employing $P_{\mu_i,t}$ as the initial guess ensures the stability of the initial closed-loop matrix $A_{cl}^0(y_{\mu_{i+1},t})$, thereby guaranteeing the convergence of the scheme. We refer to this approach as the *cascade-Newton-Kleinman* (C-NK) method, which is summarized in Algorithm 2. This concept can be extended to

consecutive time instances for a fixed parameter μ . Specifically, given $t_i < t_{i+1}$, we can use P_{μ, t_i} as initial guess when solving for $P_{\mu, t_{i+1}}$. In Section 3, theoretical justifications for selecting the distance between μ_i and μ_{i+1} (or t_i and t_{i+1}) are provided. This section explores technical aspects that, while not essential for all readers, provide valuable insights into the underlying methodology. Readers primarily interested in the main DLRA-based results and their implications may proceed directly to Section 4 without any loss of continuity.

Algorithm 2 The C-NK algorithm

Input: $A(\cdot)$, F , Q , tolerance tol , initial guess $P_{\mu_1, t}^0$, ordered set $\mathcal{P}_h = \{\mu_k\}_{k=1}^p$

Output: $P_{\mu, t}$ for all $\mu \in \mathcal{P}_h$

- 1: **for** $k = 1, \dots, p$ **do**
 - 2: $P_{\mu_k, t} = \text{NK}(A(\cdot), F, Q, \text{tol}, P_{\mu_k, t}^0)$
 - 3: $P_{\mu_{k+1}, t}^0 = P_{\mu_k, t}$
 - 4: **end for**
-

3. SENSITIVITY ESTIMATES

In this section, we derive sensitivity estimates within the SDRE framework to provide a theoretical foundation for the cascade approach. For enhanced readability, all auxiliary results required for these estimates and their numerical validation are presented in Appendix A. Section 3.1 outlines the definitions, assumptions, and established results that form the basis for deriving the sensitivity estimates of interest. In Section 3.2, we propose the sensitivity estimates related to the employment of the cascade information in the parametric space, while Section 3.3 deals with the cascade estimates for time evolution.

3.1. Preliminary notions. In the following, we provide some preliminary notions that will be necessary to the proposed sensitivity estimates. Let us consider a generic parametric dynamical system:

$$(3.1) \quad \begin{cases} \dot{y}(t; \mu) = f(t, y), \\ y(0) = y_0(\mu). \end{cases}$$

In this setting, the one-sided Lipschitz condition ensures a controlled behavior under perturbations in the parametric space and in time and represents an essential tool for the following arguments.

Definition 3.1. *A vector field $f(t, y)$ satisfies a one-sided Lipschitz condition in a domain $\Omega \subset \mathbb{R}^d$ if there exists a constant $L \in \mathbb{R}$ such that*

$$(3.2) \quad (f(t, y_1) - f(t, y_2)) \cdot (y_1 - y_2) \leq L \|y_1 - y_2\|^2, \quad \forall t \in \mathbb{R}^+, \forall y_1, y_2 \in \Omega.$$

Notably, the one-sided Lipschitz constant L differs from the standard Lipschitz constant since it can be negative. This distinction is fundamental, as the sign of L plays a key role in determining whether the system is dissipative, which is expected in a controlled problem.

In the linear case, the notion of one-sided Lipschitz constant is equivalent to the logarithmic norm, introduced in the next definition.

Definition 3.2. *Given a matrix $A \in \mathbb{C}^{d \times d}$, the logarithmic norm of the matrix A is defined as defined as*

$$(3.3) \quad \text{logm}(A) = \sup_{x \in \mathbb{C}^d \setminus \{0\}} \frac{\text{Re}((Ax) \cdot x)}{\|x\|^2},$$

where $\text{Re}(z)$ indicates the real part of $z \in \mathbb{C}$.

The logarithmic norm is a crucial tool in the stability analysis of both continuous and discrete linear dynamical systems. Specifically, since it can be demonstrated that $\|e^{tA}\| \leq e^{t \text{logm}(A)}$ for all $t \geq 0$ (see, for example, [37]), we can assert that the dynamical system is stable if $\text{logm}(A) \leq 0$.

Throughout this section, we consider the following assumptions:

- (1) The matrix function $A_{cl}(y) = A(y) - FP(y)$ is Lipschitz continuous in $\Omega \subset \mathbb{R}^d$ with Lipschitz constant $L_{cl} > 0$, i.e.,

$$(3.4) \quad \|A_{cl}(x) - A_{cl}(y)\| \leq L_{cl}\|x - y\|.$$

- (2) The pair $(A(x), B)$ is stabilizable for every $x \in \Omega \subset \mathbb{R}^d$.
(3) The pair $(A(x), Q^{1/2})$ is detectable for every $x \in \Omega \subset \mathbb{R}^d$.
(4) The function $y_0(\mu) : \mathcal{P} \subset \mathbb{R}^p \rightarrow \mathbb{R}^d$ is Lipschitz continuous with Lipschitz constant $L_{y_0} > 0$.
(5) The matrix function $A(y)$ is Lipschitz continuous in $\Omega \subset \mathbb{R}^d$ with Lipschitz constant $L_A > 0$.

For the estimates, we consider the solutions of two SDREs, defined by the pairs (μ, t) and $(\tilde{\mu}, \tilde{t})$ as

$$(3.5) \quad A_{\mu,t}^\top P_{\mu,t} + P_{\mu,t} A_{\mu,t} - P_{\mu,t} F P_{\mu,t} + Q = 0,$$

and

$$(3.6) \quad A_{\tilde{\mu},\tilde{t}}^\top P_{\tilde{\mu},\tilde{t}} + P_{\tilde{\mu},\tilde{t}} A_{\tilde{\mu},\tilde{t}} - P_{\tilde{\mu},\tilde{t}} F P_{\tilde{\mu},\tilde{t}} + Q = 0,$$

where $A_{\mu,t} = A(y(t; \mu))$ and $P_{\mu,t} = P(y(t; \mu))$, using the same notation introduced in Section 2. For both estimates, in the parametric space and time domains, we utilize a foundational result derived from Lemma 3.1 in [14] and Theorem 2.4 in [20]. Indeed, denoting the perturbation $A_{\mu,t} - A_{\tilde{\mu},\tilde{t}}$ as $\Delta A_{\mu,\tilde{\mu},t,\tilde{t}}$, the following theorem holds.

Theorem 3.3. *Suppose (3.5) has a unique positive semidefinite solution $P_{\mu,t}$. Let us assume that the perturbation $\Delta A_{\mu,\tilde{\mu},t,\tilde{t}}$ is such that*

$$(3.7) \quad \|\Delta A_{\mu,\tilde{\mu},t,\tilde{t}}\| \leq \frac{1}{2\|H_{\mu,t}\|},$$

where $H_{\mu,t}$ is the solution of the following Lyapunov equation

$$(3.8) \quad (A_{\mu,t} - F P_{\mu,t})^\top H_{\mu,t} + H_{\mu,t} (A_{\mu,t} - F P_{\mu,t}) = -I.$$

Then (3.6) has a unique symmetric nonnegative definite solution $P_{\tilde{\mu},\tilde{t}}$ and $A_{\tilde{\mu},\tilde{t}} - F P_{\mu,t}$ is stable.

In the next section, we aim to demonstrate that, under specific conditions, the Riccati equation approximation for a given parameter μ also serves as a stabilizing solution for a different parameter $\tilde{\mu}$, for a fixed time.

3.2. Cascade sensitivity estimates in the parameter space. In the C-NK approach, we first approximate the SDRE for the first parameter of a finite parametric set $\mathcal{P}_h \subset \mathcal{P}$ and then use it as an initial guess for the next SDRE approximation via the NK method. Suppose that \mathcal{P}_h is obtained by discretizing \mathcal{P} with a uniform stepsize $\Delta\mu$. We now apply the concepts introduced in Section 3.1 to the C-NK framework, deriving a criterion for selecting $\Delta\mu$ that ensures the stabilizability of the closed-loop matrix at the initial time. Furthermore, under a suitable assumption on the one-sided Lipschitz constant, this result can be extended to the entire time interval, thereby guaranteeing the convergence of the C-NK algorithm over time. For simplicity, we restrict our focus to one-dimensional parameter spaces. However, the proofs readily generalize to multidimensional cases.

Now, we can prove the following Proposition, which provides the justification of using the cascade information in the NK procedure. The auxiliary results needed for the proof are provided in Appendix A.

Proposition 3.4. *At the initial time, given $\mu \in \mathcal{P}$ and $\tilde{\mu} = \mu + \Delta\mu$, if the parameter stepsize is chosen such that*

$$(3.9) \quad \Delta\mu \leq \frac{1}{2L_A L_{y_0} \|H_{\mu,t}\|},$$

then $A_{\tilde{\mu},0} - FP_{\mu,0}$ is stable. Moreover, if

$$(3.10) \quad L \leq -\frac{1}{t} \log(2L_A L_{y_0} \Delta \mu \|H_{\mu,t}\|), \quad t \in (0, T],$$

then $A_{\tilde{\mu},t} - BP_{\mu,t}$ is stable for all $t \in [0, T]$.

Finally, provided that (3.9) and (3.10) hold, the Newton-Kleinman sequence $\{P_{\tilde{\mu},t}^j\}_j$ arising from the resolution of (2.9) with initial guess $P_{\mu,t}$ converges to the unique solution of the SDRE (3.6) for all $t \in [0, T]$.

Proof. By assumption (5) and Corollary A.3 we have

$$\|\Delta A_{\mu,\tilde{\mu},t,t}\| \leq L_A \|y(t;\mu) - y(t;\tilde{\mu})\| \leq L_A L_{y_0} \|\mu - \tilde{\mu}\| e^{Lt} = L_A L_{y_0} \Delta \mu e^{Lt}.$$

Condition (3.7) is satisfied if

$$(3.11) \quad L_A L_{y_0} \Delta \mu e^{Lt} \leq \frac{1}{2\|H_{\mu,t}\|}.$$

Condition (3.9) is obtained by imposing $t = 0$ in (3.11), while condition (3.10) is obtained manipulating (3.11) for $t > 0$. The convergence of the Newton-Kleinman sequence follows from Theorem 2.4, under assumptions (2) and (3), with the additional observation that the initial guess $P_{\mu,t}$ is such that $A_{\tilde{\mu},t} - FP_{\mu,t}$ is stable.

Remark 3.5. *Similar results can be obtained substituting the solution $y(t;\mu)$ with an approximation $\tilde{y}(t;\mu)$ of order p satisfying $\|y(t;\mu) - \tilde{y}(t;\mu)\| \leq C(\Delta t)^p$. Indeed, since*

$$(3.12) \quad \|\tilde{y}(t;\mu) - \tilde{y}(\tilde{t};\tilde{\mu})\| \leq \|y(t;\mu) - y(\tilde{t};\tilde{\mu})\| + 2C(\Delta t)^p,$$

the matrix perturbation can be bounded as

$$(3.13) \quad \|\Delta A_{\mu,\tilde{\mu},t,t}\| \leq L_A \|\tilde{y}(t,\mu) - \tilde{y}(t,\tilde{\mu})\| \leq L_A (L_{y_0} \|\mu - \tilde{\mu}\| e^{Lt} + 2C(\Delta t)^p),$$

and thus, condition (3.10) becomes

$$(3.14) \quad L \leq \frac{1}{t} [\log(1 - C(\Delta t)^p L_A \|H_{\mu,t}\|) - \log(2L_A L_{y_0} \Delta \mu \|H_{\mu,t}\|)], \quad t \in (0, T].$$

□

3.3. Cascade sensitivity estimates in time. The sensitivity estimates over the parametric space can also be extended to the time variable. We want to prove that the solution $P_{\mu,t}$ to (3.5) at time instance t is stabilizing for the Riccati equation (3.6) with $\tilde{t} = t + \Delta t$, for a proper timestep Δt and a fixed parameter μ (i.e., $\mu = \tilde{\mu}$). We aim to apply Theorem 3.3 to derive a criterion for appropriately selecting the timestep Δt in order to guarantee a stabilizing guess for the NK algorithm in time. This result is formalized in Proposition 3.6. The auxiliary results needed to prove this statement are detailed in Appendix A.

Proposition 3.6. *Assuming that*

$$\log m(A_{cl}(y)) + \log m((\nabla A_{cl}(y))y) < 0,$$

if the timestep Δt for a given parameter μ is selected to satisfy the condition

$$(3.15) \quad \Delta t \leq \frac{1}{2L_A \|A_{cl}(y_{\mu,0})y_{\mu,0}\| \|H_{\mu,t}\|},$$

then $A_{\mu,t+\Delta t} - FP_{\mu,t}$ is stable.

Finally, provided that (3.15) holds, the Newton-Kleinman sequence $\{P_{\mu,t+\Delta t}^j\}_j$ arising from the resolution of (2.9) with initial guess $P_{\mu,t}$ converges to the unique solution of the SDRE (3.6).

Proof. We define $\Delta y(t) = y_{\mu,t+\Delta t} - y_{\mu,t}$. We know that it holds

$$\|\Delta y(t)\| \leq e^{Lt} \|\Delta y(0)\| = e^{Lt} \|y_{\mu,\Delta t} - y_{\mu,0}\| \leq e^{Lt} \int_0^{\Delta t} \|A_{cl}(y_{\mu,s}) y_{\mu,s}\| ds \leq \Delta t e^{Lt} M_{\mu,\Delta t},$$

where $M_{\mu,\Delta t} = \max_{\bar{t} \in [0, \Delta t]} \|A_{cl}(y(\bar{t}, \mu)) y(\bar{t}, \mu)\|$. By Proposition A.4 we have $M_{\mu,\Delta t} = \|A_{cl}(y_{\mu,0}) y_{\mu,0}\|$, while by assumption (5) we have

$$\|\Delta A_{\mu,\mu,t,\bar{t}}\| \leq L_A \|\Delta y(t)\| \leq L_A \Delta t e^{Lt} M_{\mu,\Delta t},$$

then condition (3.7) is satisfied if condition (3.15) holds. The proof of the convergence of the Newton-Kleinman sequence relies on similar arguments as those presented in Proposition 3.3 and is therefore omitted. \square

Remark 3.7. *Similar results can be obtained by substituting the solution $y(t; \mu)$ with an approximation $\tilde{y}(t; \mu)$ of order p , using the same arguments of Remark 3.5. Indeed, assuming (3.12), when selecting the timestep Δt , we obtain*

$$\|\Delta A_{\mu,\mu,t,\bar{t}}\| \leq L_A \Delta t (e^{Lt} M_{\mu,\Delta t} + 2C(\Delta t)^{p-1}),$$

then, under the assumptions $\Delta t < 1$ and $p \geq 1$, condition (3.15) becomes

$$\Delta t \leq \frac{1}{2L_A(M_{\mu,\Delta t} + 2C)\|H_{\mu,t}\|}.$$

4. DYNAMICAL LOW RANK APPROXIMATION FOR FEEDBACK CONTROL

This section focuses on the application of the DLRA in the feedback control setting. We start from the basics of this approach in Section 4.1, and, then, we specialize the results to semilinear parametric infinite horizon optimal control problems in Section 4.2.

4.1. System decomposition and tangent spaces. Let us suppose we want to solve the parametric system (2.2), for a fixed set of parameters $\{\mu_j\}_{j=1}^p \subset \mathcal{P}$, for j and p in \mathbb{N} . For a *sampled* initial condition matrix $\mathcal{Y}_0(\mu) = [y_0^{\mu_1}, \dots, y_0^{\mu_p}] \in \mathbb{R}^{N_h \times p}$, we aim at finding $\mathcal{Y} = \mathcal{Y}(\mu) \in \mathcal{C}^1((0, \infty), \mathbb{R}^{N_h \times p})$ such that

$$(4.1) \quad \begin{cases} \dot{\mathcal{Y}}(t) = \mathcal{F}(\mathcal{Y}(t)) + BU(\mathcal{Y}(t)) & \text{for } t \in (0, \infty), \\ \mathcal{Y}(0) = \mathcal{Y}_0(\mu), \end{cases}$$

where $U : \mathbb{R}^{N_h \times p} \rightarrow \mathbb{R}^{m \times p}$ is the *control matrix*, $B \in \mathbb{R}^{N_h \times m}$ and $\mathcal{F}(\mathcal{Y}(t)) = [f(y(t; \mu_1)), \dots, f(y(t; \mu_p))] \in \mathbb{R}^{N_h \times p}$. In other terms, we recast the parametric problem (2.2), considering the dynamics for a set of p parameters *simultaneously*. The main objective is to represent the high-dimensional solution $\mathcal{Y}(t)$ in a reduced space framework of dimension $r \ll N_h$ as follows:

$$(4.2) \quad \mathcal{Y}(t) \approx \mathbf{Y} = \mathbf{U}\mathbf{Z}^\top = \sum_{i=1}^r U_i(t) Z_i(t; \mu),$$

where $\mathbf{U} = [U_1(t) | \dots | U_r(t)] \in \mathbb{R}^{N_h \times r}$ and $\mathbf{Z} \in \mathbb{R}^{p \times r}$ with $Z_{ji}(t) = Z_i(t; \mu_j)$. Furthermore, \mathbf{U} has orthonormal columns, i.e., $\mathbf{U}^\top \mathbf{U} = \mathbf{I}_r$, where \mathbf{I}_r is the identity matrix of dimension r . In other words, we represent the reduced solution in the manifold

$$(4.3) \quad \mathcal{M}_r = \{\mathbf{Y} \in \mathbb{R}^{N_h \times p} : \mathbf{Y} = \mathbf{U}\mathbf{Z}^\top, \mathbf{U}^\top \mathbf{U} = \mathbf{I}_r, \mathbf{U} \in \mathbb{R}^{N_h \times r}, \mathbf{Z} \in \mathbb{R}^{p \times r}\}.$$

The representation (4.2) is unique up to a rotation via an orthonormal matrix (see, e.g., [24]). Thus, as an alternative to the non-unique decomposition (4.2), the DLRA looks for a unique representation of the *tangent space* of (4.3) at $\mathbf{Y} = \mathbf{U}\mathbf{Z}^\top$ [24, 34], defined as

$$(4.4) \quad T_{\mathbf{Y}} \mathcal{M}_r = \{\dot{\mathbf{Y}} \in \mathbb{R}^{N_h \times p} : \dot{\mathbf{Y}} = \dot{\mathbf{U}}\mathbf{Z}^\top + \mathbf{U}\dot{\mathbf{Z}}^\top, \dot{\mathbf{U}} \in \mathbb{R}^{N_h \times r}, \dot{\mathbf{Z}} \in \mathbb{R}^{p \times r}, \mathbf{U}^\top \dot{\mathbf{U}} \in \text{so}(r)\},$$

where $\text{so}(r)$ is the space of the skew-symmetric real matrices in $\mathbb{R}^{r \times r}$.

However, the definition of this tangent space is still not unique. To guarantee a unique representation of the tangent space (4.4), we further assume an orthogonality constraint on \mathbf{U} , i.e., $\mathbf{U}^\top \dot{\mathbf{U}} = 0$. Thanks to this further assumption, with simple algebraic manipulation, we can provide the following differential equations for \mathbf{U} and \mathbf{Z} [16, 30]:

$$(4.5) \quad \begin{cases} \dot{\mathbf{U}} = (\mathbf{I}_{N_h} - \mathbf{U}\mathbf{U}^\top) \dot{\mathbf{Y}} \mathbf{Z} \mathbf{C}^{-1}, \\ \dot{\mathbf{Z}} = \dot{\mathbf{Y}}^\top \mathbf{U}, \end{cases}$$

where $\mathbf{C} = \mathbf{Z}^\top \mathbf{Z}$.

4.2. Differential equations for the reduced representation. In this section, we formalize the reduction of the infinite horizon feedback control problem, as introduced in Section 2, using the DLRA methodology.

The aim is to provide an initial decomposition for $\mathbf{Y}_0 = \mathbf{U}_0 \mathbf{Z}_0^\top$ and to evolve it in time. First, we perform an SVD on the initial datum $\mathcal{Y}_0(\mu)$. The matrix \mathbf{U}_0 is the matrix formed by the first r left singular vectors of $\mathcal{Y}_0(\mu)$, while the coefficient matrix is given by $\mathbf{Z}_0 = \mathcal{Y}_0^\top \mathbf{U}_0$. In our setting, we exploit the definition of the system (4.1) approximated by

$$(4.6) \quad \begin{cases} \dot{\mathbf{Y}} = \mathcal{F}(\mathbf{Y}) + \mathbf{B}\mathbf{U}(\mathbf{Y}), \\ \mathbf{Y}(0) = \mathbf{Y}_0. \end{cases}$$

Substituting the reduced dynamics (4.6) into equation (4.5), we obtain

$$(4.7) \quad \begin{cases} \dot{\mathbf{U}} = (\mathbf{I}_{N_h} - \mathbf{U}\mathbf{U}^\top) (\mathcal{F}(\mathbf{U}\mathbf{Z}^\top) + \mathbf{B}\mathbf{U}(\mathbf{U}\mathbf{Z}^\top)) \mathbf{Z} \mathbf{C}^{-1}, \\ \dot{\mathbf{Z}} = (\mathcal{F}(\mathbf{U}\mathbf{Z}^\top) + \mathbf{B}\mathbf{U}(\mathbf{U}\mathbf{Z}^\top))^\top \mathbf{U}. \end{cases}$$

We now want (i) to derive a feedback law for the control matrix $\mathcal{U}(\cdot)$ and (ii) to establish a specific low rank and efficient representation of (4.7) when $f(y) = \mathbf{A}y + \mathbf{T}(y \otimes y)$, where $\mathbf{A} \in \mathbb{R}^{N_h \times N_h}$ and $\mathbf{T} \in \mathbb{R}^{N_h \times N_h^2}$.

This is the case of the numerical results presented in Section 6. Nevertheless, this approach can be readily extended to polynomial nonlinearities; however, we note that quadratic nonlinearities are prevalent in many applications.

Let us start with (i) the definition of the feedback law. By transposing the equation for \mathbf{Z} and denoting $\tilde{\mathbf{Z}} = \mathbf{Z}^\top$, we obtain for each parameter μ_j

$$\dot{\tilde{\mathbf{Z}}}_j = \mathbf{U}^\top \mathbf{A} \mathbf{U} \tilde{\mathbf{Z}}_j + \mathbf{U}^\top \mathbf{T}((\mathbf{U} \tilde{\mathbf{Z}}_j) \otimes (\mathbf{U} \tilde{\mathbf{Z}}_j)) + \mathbf{U}^\top \mathbf{B} \mathcal{U}_j,$$

where $\tilde{\mathbf{Z}}_j$ denotes the j -th column of $\tilde{\mathbf{Z}}$ and \mathcal{U}_j denotes the control associated with the dynamical system for the parameter μ_j . Utilizing the property $(\mathbf{A}\mathbf{B}) \otimes (\mathbf{C}\mathbf{D}) = (\mathbf{A} \otimes \mathbf{C})(\mathbf{B} \otimes \mathbf{D})$, we obtain

$$(4.8) \quad \dot{\tilde{\mathbf{Z}}}_j = \mathcal{A}_r \tilde{\mathbf{Z}}_j + \mathcal{T}_r(\tilde{\mathbf{Z}}_j \otimes \tilde{\mathbf{Z}}_j) + \mathcal{B}_r \mathcal{U}_j,$$

where¹ $\mathcal{A}_r = \mathbf{U}^\top \mathbf{A} \mathbf{U} \in \mathbb{R}^{r \times r}$, $\mathcal{T}_r = \mathbf{U}^\top \mathbf{T}(\mathbf{U} \otimes \mathbf{U}) \in \mathbb{R}^{r \times r^2}$ and $\mathcal{B}_r = \mathbf{U}^\top \mathbf{B} \in \mathbb{R}^{r \times m}$. Equation (4.8) can be written in the following semilinear form

$$(4.9) \quad \dot{\tilde{\mathbf{Z}}}_j = \mathcal{A}_r(\tilde{\mathbf{Z}}_j) \tilde{\mathbf{Z}}_j + \mathcal{B}_r \mathcal{U}_j,$$

where

$$(\mathcal{A}_r(H))(i, j) = \mathcal{A}_r(i, j) + \sum_{k=1}^r \mathcal{T}_r(i, (j-1)r + k) H_k, \quad i, j \in \{1, \dots, r\},$$

for $H \in \mathbb{R}^r$. The cost functional (2.1) in the reduced framework reads as

$$(4.10) \quad \min_{\mathcal{U}_j(\cdot) \in \mathcal{U}_{ad}} J_r(\mathcal{U}_j(\cdot), \tilde{\mathbf{Z}}_j(0)) = \int_0^\infty \tilde{\mathbf{Z}}_j(s)^\top \mathcal{Q}_r \tilde{\mathbf{Z}}_j(s) + \mathcal{U}_j(s)^\top \mathcal{R} \mathcal{U}_j(s) ds,$$

¹For the sake of notation, we disregard the dependence of the matrices on the basis \mathbf{U} .

with $Q_r = \mathbf{U}^\top \mathbf{Q} \mathbf{U} \in \mathbb{R}^{r \times r}$. Given the dynamics (4.9) and the cost functional (4.10), the associated SDRE reads

$$(4.11) \quad \mathcal{A}_r(\tilde{\mathbf{Z}}_j)^\top P(\tilde{\mathbf{Z}}_j) + P(\tilde{\mathbf{Z}}_j) \mathcal{A}_r(\tilde{\mathbf{Z}}_j) - P(\tilde{\mathbf{Z}}_j) F_r P(\tilde{\mathbf{Z}}_j) = Q_r,$$

where $P(\tilde{\mathbf{Z}}_j) \in \mathbb{R}^{r \times r}$ and $F_r = B_r R^{-1} B_r^\top \in \mathbb{R}^{r \times r}$. Upon solving the SDRE, the feedback control can be determined as

$$\mathbf{U}_j = -R^{-1} B_r^\top P(\tilde{\mathbf{Z}}_j) \tilde{\mathbf{Z}}_j.$$

With the feedback representation for the control matrix \mathbf{U} established, our objective is (ii) to efficiently and compactly describe the dynamics in (4.7). Let $P_{\tilde{\mathbf{Z}}} \in \mathbb{R}^{r \times p}$ be a matrix with columns defined by

$$(P_{\tilde{\mathbf{Z}}})(:, j) = P(\tilde{\mathbf{Z}}_j) \tilde{\mathbf{Z}}_j, \quad j = 1, \dots, p.$$

Then,

$$\mathbf{U}^\top (B\mathbf{U}) = -B_r R^{-1} B_r^\top P_{\tilde{\mathbf{Z}}} = -F_r P_{\tilde{\mathbf{Z}}}.$$

Additionally, we can express

$$B\mathbf{U}\mathbf{Z} = -B R^{-1} B_r^\top P_{\tilde{\mathbf{Z}}} \tilde{\mathbf{Z}}^\top = -S(\tilde{\mathbf{Z}}).$$

Substituting these expressions, we obtain the following DLRA equations:

$$(4.12) \quad \begin{cases} \dot{\mathbf{U}} = F_{\mathbf{U}}(\mathbf{U}, \tilde{\mathbf{Z}}) = (I_{N_h} - \mathbf{U}\mathbf{U}^\top)(A\mathbf{U} + T(\mathbf{U} \otimes \mathbf{U})V(\tilde{\mathbf{Z}}) - W(\tilde{\mathbf{Z}})), \\ \dot{\tilde{\mathbf{Z}}} = F_{\tilde{\mathbf{Z}}}(\mathbf{U}, \tilde{\mathbf{Z}}) = A_r \tilde{\mathbf{Z}} + T_r V_{\otimes}(\tilde{\mathbf{Z}}) - F_r(\mathbf{U}) P_{\tilde{\mathbf{Z}}}, \end{cases}$$

where

$$V(\tilde{\mathbf{Z}}) = V_{\otimes}(\tilde{\mathbf{Z}}) \tilde{\mathbf{Z}}^\top \mathbf{C}^{-1} \in \mathbb{R}^{r^2 \times r}, \quad V_{\otimes}(\tilde{\mathbf{Z}}) = [\tilde{\mathbf{Z}}_1 \otimes \tilde{\mathbf{Z}}_1, \dots, \tilde{\mathbf{Z}}_p \otimes \tilde{\mathbf{Z}}_p] \in \mathbb{R}^{r^2 \times p},$$

and

$$W(\tilde{\mathbf{Z}}) = F_r(P_{\tilde{\mathbf{Z}}} \tilde{\mathbf{Z}}^\top) \mathbf{C}^{-1} \in \mathbb{R}^{N_h \times r}.$$

In equations (4.12), we separate the terms that depend on \mathbf{U} from those that depend on $\tilde{\mathbf{Z}}$. This partitioning ensures that the computational cost remains independent of the original dimension $N_h \times p$.

Remark 4.1. *Let us point out that the numerical approximation of the system (4.12) must keep the orthogonality condition for \mathbf{U} for all times t . This can be achieved in two ways (see, e.g., [16]):*

- *integrating the equation (4.12) via a classical method and then we apply a QR factorization on the new iterate for \mathbf{U} ,*
- *applying numerical integration methods able to preserve the orthogonality.*

We adopt the second approach, drawing on the framework established in [5], where the authors introduce an intrinsic numerical method designed to preserve the geometric structure of the orthogonal Stiefel manifold, defined as the set of $N_h \times r$ matrices with orthonormal columns. The proposed algorithm achieves a computational complexity of $O(N_h r^2)$, highlighting its efficiency and reliability, and automatically preserves the orthogonality condition for \mathbf{U} .

5. NUMERICAL ALGORITHMS

In this section, we present the final algorithms, which incorporate the elements introduced in the previous sections. In Section 5.1, we recall the basics principles of the POD approach, i.e., the most well-established strategy used to perform model order reduction in this context. In Section 5.2, we introduce the DLRA combined with the C-NK approach to solve the SDRE. In Section 5.3, we propose the Riccati-based DLRA (R-DLRA) strategies, which guarantee an increased accuracy with respect to the standard DLRA approach counterpart, as we will further discuss in Section 6.

5.1. Proper Orthogonal Decomposition. This section describes the basic aspects of the POD for nonlinear feedback control. The application of POD within this context is detailed in Algorithm 3, where the POD is combined with the \mathbf{C} -NK method with cascade information both in the parameters and in time (lines 6, 7, and 10 of Algorithm 3). The POD approach relies on the construction of fixed basis functions based on an initial computation of the FOM controlled dynamics, called *snapshots*, for a selected subset of parameters $\overline{\mathcal{P}}_h \subset \mathcal{P}$ with cardinality $|\overline{\mathcal{P}}_h| = \overline{p}$ and time instances $\{\overline{t}_i\}_{i=1}^{\overline{N}_T}$. More precisely, let us consider a set of solution snapshots denoted as $\{y(t_i; \mu_j), i = 1, \dots, \overline{N}_T, j = 1, \dots, \overline{p}\}$, and define the corresponding snapshot matrix as

$$(5.1) \quad S = [y(t_1; \mu_1), \dots, y(t_{\overline{N}_T}; \mu_1), y(t_1; \mu_2), \dots, y(t_{\overline{N}_T}; \mu_{\overline{p}})] \in \mathbb{R}^{N_h \times N_s},$$

with $N_s = \overline{N}_T \cdot \overline{p}$. A POD basis of dimension $r \leq N_s$ is constructed by performing an orthogonal reduction of the matrix S . Specifically, given the Singular Value Decomposition (SVD) of S , we obtain

$$S = V \Sigma W^T, \quad V, W \in \mathbb{R}^{N_h \times N_s}, \Sigma \in \mathbb{R}^{N_s \times N_s}.$$

The POD basis matrix $V_r = [v_1 | \dots | v_r] \in \mathbb{R}^{N_h \times r}$ contains the first r left singular vectors corresponding to the r largest singular values. Given a tolerance tol , the value of r is determined to satisfy the following criterion:

$$(5.2) \quad \frac{\sum_{i=1}^r \sigma_i^2}{\sum_{i=1}^{\min(N_h, p)} \sigma_i^2} > \text{tol},$$

where $\{\sigma_i\}_{i=1}^{\min(N_h, p)}$ are the singular values of the SVD decomposition. Using the reduced basis matrix V_r , the state vector $y_{\mu, t}$ can be approximated as $y_{\mu, t} \approx V_r y_{\mu, t}^r$, where $y_{\mu, t}^r \in \mathbb{R}^r$ is the solution of the following reduced dynamical system

$$(5.3) \quad \dot{y}_r(t; \mu) = A_r y_{\mu, t}^r + T_r (y_{\mu, t}^r \otimes y_{\mu, t}^r) + B_r u(y_{\mu, t}^r),$$

where $A_r = V_r^T A V_r \in \mathbb{R}^{r \times r}$, $T_r = V_r^T T (V_r \otimes V_r) \in \mathbb{R}^{r \times r^2}$ and $B_r = V_r^T B \in \mathbb{R}^{r \times m}$. We recall that the peculiar quadratic structure (5.3) allows an efficient representation of the reduced system [11, 33]. As in the previous section, the reduced system (5.3) can also be expressed in semilinear form as in (4.9), while the cost functional is similarly reduced to the form in (4.10), with $Q_r = V_r^T Q V_r$. Notice that the reduced basis V_r is fixed: it is precomputed offline and subsequently, the reduced system is assembled and solved for a new parametric instance, in an online phase.

Algorithm 3 The POD algorithm

Input: $\mathcal{A}_r(\cdot), F, Q$, initial conditions \mathcal{Y}_0 , initial guess P_r^0 , ordered training set $\overline{\mathcal{P}}_h$, ordered set ordered training set $\mathcal{P}_h = \{\mu_k\}_{k=1}^{\overline{p}}$, training time discretization $\{\overline{t}_i\}_{i=1}^{\overline{N}_T}$, time discretization $\{t_i\}_{i=1}^{\overline{N}_T}$

Output: controlled solutions $\{y_{\mu, t_i}^r\}_{\mu, i}$

- 1: Compute the snapshot matrix S
 - 2: Perform an SVD of the matrix S and build the POD basis V_r
 - 3: Build **once and for all** all the reduced matrices
 - 4: **for** $i = 1, \dots, \overline{N}_T - 1$ **do**
 - 5: **for** $\mu \in \overline{\mathcal{P}}_h$ **do**
 - 6: $P_{\mu, t_i} = \text{NK}(\mathcal{A}_r(\cdot), F_r, Q_r, \text{tol}, P_r^0)$
 - 7: $P_r^0 = P_{\mu, t_i}$
 - 8: Integrate (5.3) in $(t_i, t_{i+1}]$
 - 9: **end for**
 - 10: $P_r^0 = P_{\mu_1, t_i}$
 - 11: **end for**
-

5.2. Standard DLRA. This section focuses on the DLRA approach for feedback control problems, leveraging the C-NK strategy to solve the SDREs efficiently during the numerical integration process. The procedure is outlined in Algorithm 4. It begins by performing an SVD of the initial condition matrix \mathcal{Y}_0 . Through this process, we obtain the matrix $\mathbf{U}_0 \in \mathbb{R}^{N_h \times r}$ and the coefficient matrix $\mathbf{Z}_0 = \mathcal{Y}_0^\top \mathbf{U}_0 \in \mathbb{R}^{r \times p}$, where p and r are the number of considered parameters and basis functions, respectively. As for the POD, the number of basis functions r is selected by means of the retained total energy criterion (5.2).

Algorithm 4 The standard DLRA algorithm

Input: $\mathcal{A}_r(\cdot), F, Q$, initial conditions \mathcal{Y}_0 , initial guess P_r^0 , ordered set \mathcal{P}_h , time discretization $\{t_i\}_{i=1}^{N_T}$
Output: controlled solutions represented as $\{\mathbf{U}(t_i)\}_{i=1}^{N_T}$ and $\{\mathbf{Z}(t_i)\}_{i=1}^{N_T}$

- 1: $\text{SVD}(\mathcal{Y}_0) \rightarrow \mathbf{U}_0$ and $\mathbf{Z}_0 = \mathbf{U}_0^\top \mathcal{Y}_0$
- 2: **for** $i = 1, \dots, N_T - 1$ **do**
- 3: Build all the reduced matrices
- 4: $\{P_{\mu, t_i}\}_{\mu \in \mathcal{P}} = \text{C-NK}(\mathcal{A}_r(\cdot), F_r, Q_r, \text{tol}, P_r^0, t_i, \mathcal{P}_h)$
- 5: Integrate (4.12) in $(t_i, t_{i+1}]$
- 6: $P_r^0 = P_{\mu_1, t_i}$
- 7: **end for**

Therefore, at each time instance, we solve p reduced parametric SDREs (4.11) using the C-NK. The cascade approach is implemented to accelerate the computation of the solution even at the reduced level, as demonstrated in Section 6. The C-NK considers the information both in the parametric space and in time, except for the very first iteration, i.e., for time t_1 and parameter μ_1 , the null matrix is employed as an initial guess. Once solved all the SDREs, we assemble the matrices in $F_{\mathbf{U}}(\mathbf{U}, \tilde{\mathbf{Z}})$ and $F_{\tilde{\mathbf{Z}}}(\mathbf{U}, \tilde{\mathbf{Z}})$ and integrate the system (4.12) using a midpoint scheme. Notably, the integration of \mathbf{U} on the manifold of unitary matrices employs a tangent scheme to ensure geometric consistency, as pointed out in Remark 4.1.

5.3. Riccati-based DLRA and POD. The DLRA algorithm considers basis functions derived from the SVD of the initial conditions and subsequently evolves them according to the dynamical system (4.12). However, it is noteworthy, that these basis functions are also used for the projection and approximation of the SDREs, even though the initial data does not contain any information related to the Riccati equations. This is not the case with POD, for example, whose construction is based on controlled snapshots based on the full dimensional SDREs. Thus, incorporating additional control-related features in the DLRA approach, such as the Riccati solution or the feedback matrix, could enhance the quality of the approximation. Motivated by the strategies outlined in [35, 36], we propose to employ the information from the Riccati solution (P) or the feedback matrix (K) to increase the accuracy of the DLRA procedure. We denote these enhanced DLRA approaches with P-DLRA and K-DLRA, respectively. We will refer to these two novel strategies as R-DLRA.

Algorithm 5 The P-DLRA algorithm

Input: $\mathcal{A}_r(\cdot), F, Q$, initial conditions \mathcal{Y}_0 , initial guess P_r^0 , ordered set \mathcal{P}_h , time discretization $\{t_i\}_{i=1}^{N_T}$, number of initial Riccati solutions s
Output: controlled solutions $\{\mathbf{U}(t_i)\}_{i=1}^{N_T}$ and $\{\mathbf{Z}(t_i)\}_{i=1}^{N_T}$

- 1: $\text{SVD}(\mathcal{Y}_0) \rightarrow \mathbf{U}_0$ and $\mathbf{U}_0^\top \mathcal{Y}_0 = \mathbf{Z}_0$
- 2: Compute $P_{\mu_j, 0}$ for $j = 1, \dots, s$ and build \mathbf{P}
- 3: $\mathbf{U}_P = \text{SVD}((I - \mathbf{U}_0 \mathbf{U}_0^\top) P_0) \rightarrow \mathbf{U}_0 = [\mathbf{U}_0, \mathbf{U}_P]$
- 4: Follow Steps 2-7 of Algorithm 4

Specifically, for the P-DLRA, once built the initial basis \mathbf{U}_0 from $\mathcal{Y}_0(\mu)$, given a fixed set of parameters $\{\mu_j\}_{j=1}^s$ uniformly distributed in \mathcal{P} , before the time integration, we compute the corresponding Riccati solutions $\{P_{\mu_j,0}\}_{j=1}^s$, and collect them in a matrix $\mathbf{P} = [P_{\mu_1,0}, \dots, P_{\mu_s,0}] \in \mathbb{R}^{N_h \times N_h \cdot s}$. At this point, the basis \mathbf{U}_0 is enriched with a basis \mathbf{U}_P , related to an SVD over $(I - \mathbf{U}_0 \mathbf{U}_0^\top) \mathbf{P}$, to guarantee the orthogonality of the new basis functions with respect to \mathbf{U}_0 . Then, the classical DLRA steps are performed in order to solve system (4.12). An analogous argument can be applied for the K-DLRA, where the initial basis functions in \mathbf{U}_0 are enriched by the basis \mathbf{U}_K built by an SVD over $(I - \mathbf{U}_0 \mathbf{U}_0^\top) \mathbf{K}$, where $\mathbf{K} = [K_{\mu_1,0}, \dots, K_{\mu_s,0}] \in \mathbb{R}^{m \times s}$ collects the feedback matrices related to the Riccati solution in \mathbf{P} , i.e., $K_{\mu_j,0} = -R^{-1} B^\top P_{\mu_j,0}$, for $j = 1, \dots, s$. The P-DLRA and K-DLRA algorithms, which detail this approach, are presented in Algorithms 5 and 6, respectively.

Algorithm 6 The K-DLRA algorithm

Input: $\mathcal{A}_r(\cdot), F, Q$, initial conditions \mathcal{Y}_0 , initial guess P_r^0 , ordered set \mathcal{P}_h , time discretization $\{t_i\}_{i=1}^{N_T}$, number of initial Riccati solutions s
Output: controlled solutions $\{\mathbf{U}(t_i)\}_{i=1}^{N_T}$ and $\{\mathbf{Z}(t_i)\}_{i=1}^{N_T}$

- 1: $\text{SVD}(\mathcal{Y}_0) \rightarrow \mathbf{U}_0$ and $\mathbf{U}_0^\top \mathcal{Y}_0 = \mathbf{Z}_0$
 - 2: Compute $K_{\mu_j,0}$ for $j = 1, \dots, s$ and build \mathbf{K}
 - 3: $\mathbf{U}_K = \text{SVD}((I - \mathbf{U}_0 \mathbf{U}_0^\top) \mathbf{K}) \rightarrow \mathbf{U}_0 = [\mathbf{U}_0, \mathbf{U}_K]$
 - 4: Follow Steps 2-7 of Algorithm 4
-

The Riccati-based approach can be employed within the POD algorithm by enriching the basis functions built from the controlled snapshots. For completeness, the P-POD and K-POD are detailed in Algorithms 7 and 8, respectively. We refer to these two strategy with the common name R-POD.

Algorithm 7 The P-POD algorithm

Input: $\mathcal{A}_r(\cdot), F, Q$, initial conditions \mathcal{Y}_0 , initial guess P_r^0 , ordered training set $\overline{\mathcal{P}_h}$, ordered set \mathcal{P}_h , training time discretization $\{\bar{t}_i\}_{i=1}^{\overline{N}_T}$, time discretization $\{t_i\}_{i=1}^{N_T}$, number of initial Riccati solutions s
Output: controlled solutions $\{y_r(t_i, \mu)\}_{i,\mu}$

- 1: Apply FOM for $t \in \{t_i\}_{i=1}^{N_T}$ and μ in $\overline{\mathcal{P}_h}$ (C-NK)
 - 2: Apply POD obtaining \mathbf{U} ($\dim=r$)
 - 3: Compute $P_{\mu_j,0}$ for $j = 1, \dots, s$ and build \mathbf{P}
 - 4: $\mathbf{U}_P = \text{SVD}((I - \mathbf{U} \mathbf{U}^\top) \mathbf{P}) \rightarrow \mathbf{U} = [\mathbf{U}, \mathbf{U}_P]$
 - 5: Follow Steps 3-11 of Algorithm 3
-

Algorithm 8 The K-POD algorithm

Input: $\mathcal{A}_r(\cdot), F, Q$, initial conditions \mathcal{Y}_0 , initial guess P_r^0 , ordered training set $\overline{\mathcal{P}_h}$, ordered set \mathcal{P}_h , training time discretization $\{\bar{t}_i\}_{i=1}^{\overline{N}_T}$, time discretization $\{t_i\}_{i=1}^{N_T}$, number of initial Riccati solutions s
Output: controlled solutions $\{y_r(t_i, \mu)\}_{i,\mu}$

- 1: Apply FOM for $t \in \{t_i\}_{i=1}^{N_T}$ and μ in $\overline{\mathcal{P}_h}$ (C-NK)
 - 2: Apply POD obtaining \mathbf{U} ($\dim=r$)
 - 3: Compute $K_{\mu_j,0}$ for $j = 1, \dots, s$ and build \mathbf{K}
 - 4: $\mathbf{U}_K = \text{SVD}((I - \mathbf{U} \mathbf{U}^\top) \mathbf{K}) \rightarrow \mathbf{U} = [\mathbf{U}, \mathbf{U}_K]$
 - 5: Follow Steps 3-11 of Algorithm 3
-

6. NUMERICAL RESULTS

This section presents numerical results comparing the DLRA and R-DLRA methods with standard POD and R-POD reduction techniques. In Section 6.1, two experiments are introduced, both centered on an optimal control problem governed by the one-dimensional Burgers' equation. In the first experiment, we demonstrate the advantages of employing C-NK strategy in comparison to `icare` (a direct Matlab solver for Riccati equations) and NK methods across FOM, DLRA, and POD frameworks. The second experiment focuses on a comparative analysis of DLRA and R-DLRA against POD and R-POD in terms of computational efficiency (measured by CPU time) and solution accuracy relative to the FOM. Section 6.2 introduces the third experiment, which extends the comparison to a two-dimensional optimal control problem constrained by the Burgers' equation. Here, the performance of DLRA and R-DLRA is evaluated against POD and R-POD, considering both computational efficiency and accuracy with respect to the FOM solution.

6.1. 1D Burgers' equation. We define the computational domain $\Omega = [-5, 30]$ and the computational time interval $I = [0, T]$, with $T = 1$. Throughout the following discussion, $\chi_\omega(\cdot)$ denotes the indicator function over the subdomain ω . The interval ω_c specifies the region where the control action is active, while ω_o indicates the interval where we observe the dynamics. At the continuous level, the optimal control problem is formulated as follows:

$$(6.1) \quad J(u, y_0) = \int_0^{+\infty} \int_{\omega_o} |y(t, x)|^2 dx + 0.1 \int_{\omega_c} |u(t, x)|^2 dx dt,$$

subject to

$$(6.2) \quad \frac{d}{dt}y(t, x) + y(t, x)\partial_x y(t, x) + 20\partial_x y(t, x) = u(t, x)\chi_{\omega_c}(x),$$

for a given parametric initial condition $y_0(x; \mu) = \mu_1 e^{-\mu_2 x^2}$ with $\mu = (\mu_1, \mu_2) \in \mathcal{P} = [0.1, 0.5] \times [0.2, 1.5]$. Homogeneous Neumann boundary conditions are imposed for $x = -5$ and $x = 30$. For the numerical discretization, a Finite Difference scheme in space is applied, resulting in a FOM of dimension $N_h = 100$. Time integration is performed using a midpoint quadrature rule with a time step of $\Delta t = 10^{-3}$. In this study, the control acts on the subdomain $\omega_c = [-1, 1] \cup [5, 7]$, while the observation is taken over $\omega_o = [2, 4] \cup [8, 10]$. The POD and R-POD models are built with a 4×4 parametric grid over \mathcal{P} , with 100 snapshots in time for each parameter, resulting in a total of $N_s = 1600$ snapshots. The DLRA and R-DLRA approaches compute the solution at all time instances using a 20×20 parametric grid over \mathcal{P} , corresponding to $p = 400$ parameters. In the C-NK setting, the parameters are ordered according to the following rule: we first vary the first parameter while keeping the second parameter fixed. Specifically, starting with $j = 1$, we consider the pairs $(\mu_1^j, \mu_2^1), \dots, (\mu_1^j, \mu_2^{20})$. Subsequently, we increment j to $j + 1$ and repeat this process until $j = 20$. This parametric grid is also used as a testing set for the POD method. The reduced dynamics for both DLRA and POD strategies are integrated consistently with the FOM. The performances are tested in terms of CPU times and L^2 absolute error in the state dynamic and the control for $t \in I$. The state and control errors are denoted by

$$E = E(t) = \frac{1}{|\mathcal{P}_h|} \sum_{\mu \in \mathcal{P}_h} \|y_{\mu,t} - y_{\mu,t}^r\|_{L^2(\Omega)} \quad \text{and} \quad E_c = E_c(t) = \frac{1}{|\mathcal{P}_h|} \sum_{\mu \in \mathcal{P}_h} \|u_{\mu,t} - u_{\mu,t}^r\|_{L^2(\omega_c)},$$

respectively, where we recall that $y_{\mu,t}^r$ represent the reduced (i.e., DLRA or POD) state solution at time t for a given μ , while $u_{\mu,t}^r$ represent the reduced (i.e., DLRA or POD) control solution at time t for a given μ , to be compared to the FOM solutions.

Experiment 1: What is the best option between `icare`, NK, and C-NK?

In this test, we investigate the performances of the Matlab function `icare`, NK scheme (Algorithm 1), and C-NK method (Algorithm 2) to solve the SDRE related to the optimal control problem of Section 6.1 both at the FOM and ROM level. For DLRA, we need to apply an SVD over the parametric initial condition $\mathcal{Y}_0(\mu) \in \mathbb{R}^{N_h \times p}$. We choose the basis functions by an energy criterion

(5.2) over the parametric initial condition, with a tolerance $\text{tol} = 0.9999$. DLRA meets the criterion for $r = 4$. For the POD, we retain the same number of basis functions for an SVD over the N_s snapshots, to be comparable to the DLRA setting.

The indicators taken into consideration for the comparison are:

- the global CPU time, i.e., the time needed to perform the simulations for the $p = 400$ parameters. For the POD, the global CPU also considers the offline phase [30]. This is a natural choice: the DLRA procedure is *on the fly* and does not need any training compared to the POD approach. Thus, the global CPU should consider the offline time which is a mandatory step for the POD;
- the CPU of NK, i.e., the CPU time, averaged in time and in the parametric space, needed to the NK-based strategies to converge;
- the average number of iterations needed to the NK-based strategies to converge;
- the average state and control error.

The results are summarized in Table 1. The initial guess for NK is consistently the trivial one (the null matrix). In contrast, C-NK utilizes the trivial guess solely at the first time instance and for the first parameter. Subsequently, it employs cascade information guided by the sensitivity analysis discussed in Section 3.

We observe that C-NK obtains the lowest global CPU for *all* the strategies. While this was quite expected at the FOM level (and consequently for the POD during the offline stage), this conclusion was not obvious for DLRA. Indeed, DLRA *only solves reduced Riccati* and direct methods, such as `icare`, can be highly competitive. However, from the table, we note that C-NK is two times faster than the direct method and slightly faster than the classical NK. Indeed, using the cascade information reduces the time of convergence of the method and the number of iterations needed for the three algorithms. In addition, for the reduced strategies, the accuracy achieved with the iterative solver is the same as the one obtained with the `icare` direct solver. Based on these results, we conclude that C-NK is the most suitable choice for the FOM, DLRA, and POD-based strategies in the subsequent experiments.

TABLE 1. Experiment 1. CPU and accuracy comparison for `icare`, NK and C-NK between FOM, DLRA and POD ($r = 4$).

	icare			NK			C-NK		
	FOM	DLRA	POD	FOM	DLRA	POD	FOM	DLRA	POD
Global CPU	$1.45 \cdot 10^4$	241	843	$1.85 \cdot 10^4$	138	748	$8.72 \cdot 10^3$	122	496
CPU of NK	-	-	-	$3.55 \cdot 10^{-2}$	$2.34 \cdot 10^{-4}$	$3.46 \cdot 10^{-4}$	$1.92 \cdot 10^{-2}$	$2.11 \cdot 10^{-4}$	$2.51 \cdot 10^{-4}$
Iterations	-	-	-	4	3.61	5	1.29	1.34	1.81
Average E	-	$1.10 \cdot 10^{-3}$	$5.10 \cdot 10^{-3}$	-	$1.10 \cdot 10^{-3}$	$5.10 \cdot 10^{-3}$	-	$1.10 \cdot 10^{-3}$	$5.10 \cdot 10^{-3}$
Average E_c	-	$3.91 \cdot 10^{-4}$	$3.10 \cdot 10^{-3}$	-	$3.91 \cdot 10^{-4}$	$3.10 \cdot 10^{-3}$	-	$3.91 \cdot 10^{-4}$	$3.10 \cdot 10^{-3}$

Experiment 2: What is the best option between DLRA, R-DLRA, POD, and R-POD?

In this test case, we investigate the role of the Riccati information in terms of CPU and the accuracy of the DLRA and the POD approaches compared to the FOM solution. The SDREs are always solved using the C-NK algorithm, which proved to be the best approach both at the FOM and ROM settings in Experiment 1. Let us start our analysis from DLRA and POD. We are working in the numerical setting of the previous test case, with $r = 4$ basis functions. In Figure 1, we compare the DLRA and POD approaches in terms of the evolution of the state error $E(t)$ and the CPU times. In the left panel the evolution of E in time is represented. For the same r , the DLRA approach provides a more accurate recovery of the FOM dynamics over time compared to the POD method. In the right panel, we fix $r = 4$ for the DLRA, leading to a final accuracy of $E(T) = 1.4 \cdot 10^{-3}$ and compare it to the accuracy of the POD method for increasing values of r . We also report

the ratio of the CPU time for DLRA to the CPU time for POD. To achieve the same accuracy as DLRA, the POD method requires $r = 10$ basis functions. However, DLRA proves to be significantly more computationally efficient, being approximately four times faster. The same conclusions can be drawn by analyzing the first column of Table 2 : DLRA emerges as the most efficient approach, demonstrating a lower CPU time and a significant *speedup* compared to the FOM. Here, *speedup* is defined as the ratio of the CPU time required by the FOM to solve the dynamics for $p = 400$ parameters to the CPU time required by the reduced-order strategy to accomplish the same task.

The superior accuracy of the DLRA approach is illustrated in Figure 2. The top plot compares the FOM, DLRA, and POD solutions averaged over \mathcal{P}_h at the final time T . While the POD method fails to accurately reconstruct the solution, the DLRA approach captures the dynamics of the FOM more effectively. However, it is noted that the magnitude of the solution is not fully recovered by the DLRA.

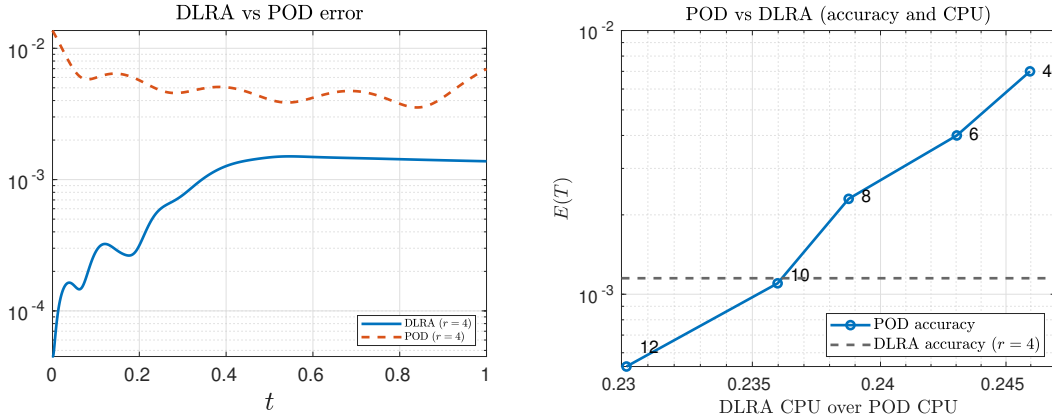


FIGURE 1. Experiment 2. *Left*: Evolution of $E(t)$ for DLRA and POD for $r = 4$. *Right*: POD final accuracy plot with CPU times for increasing values of r to be compared to the final accuracy of the DLRA.

We overcome this issue thanks to the R-DLRA approaches. When working with Riccati-based strategies, we work with $r = r_1 + r_2$ basis functions, where r_1 is the number of basis functions retained by the SVD of the initial state, i.e., $r_1 = 4$, while r_2 is the number of additional bases related to the Riccati information computed on the same p parameters used to compute $\mathcal{Y}_0(\mu)$. In the case of K-DLRA, $r_2 = 5$ retains the 0.9999 of the energy, while for P-DLRA, to retain the same amount of energy, $r_2 = 19$ is needed, leading to a global basis number of $r = 9$ and $r = 23$ for the two approaches, respectively. From the bottom row of Figure 2, we see that adding Riccati bases is undoubtedly beneficial for the DLRA. By employing this approach, we closely track the dynamics of the system, achieving a visual overlap between the FOM and the P-DLRA profiles. This is not the case for K-POD and P-POD: the Riccati information yields spurious oscillations in the solution. In Figure 3, the top panel shows that P-POD improves the accuracy of the solution compared to K-POD and standard POD (as indicated by the red dashed line in the left plot of Figure 1). However, P-POD provides a less accurate representation of the FOM solution when compared to P-DLRA (it is even less accurate than K-DLRA). In the same figure, in the middle and bottom plots, we propose the performance analysis in terms of accuracy and CPU times. In the left plots, we fix r for the K-DLRA and P-DLRA, while we fix $r_1 = 4$ and we increase r_2 for the R-POD. It is evident that adding more Riccati-based bases does not improve the accuracy of the POD method. The only way to reduce the error is to fix r_2 ($r_2 = 5$ and $r_2 = 19$ for K-POD and P-POD, respectively) and increase r_1 . Once again, while R-POD strategies can achieve the same accuracy as their R-DLRA counterparts, they require significantly more computational time. Specifically, K-DLRA is nearly three times faster than K-POD, and P-DLRA is approximately two times faster than P-POD.

Table 2 summarizes the CPU time for the Riccati-based strategies. Once again, K-DLRA and P-DLRA outperform their respective POD counterparts. While P-DLRA demonstrates superior accuracy in capturing the model dynamics, it does so at the cost of increased computational time, as expected. Nevertheless, DLRA, K-DLRA, and P-DLRA consistently require less computational time compared to their corresponding POD-based approaches.

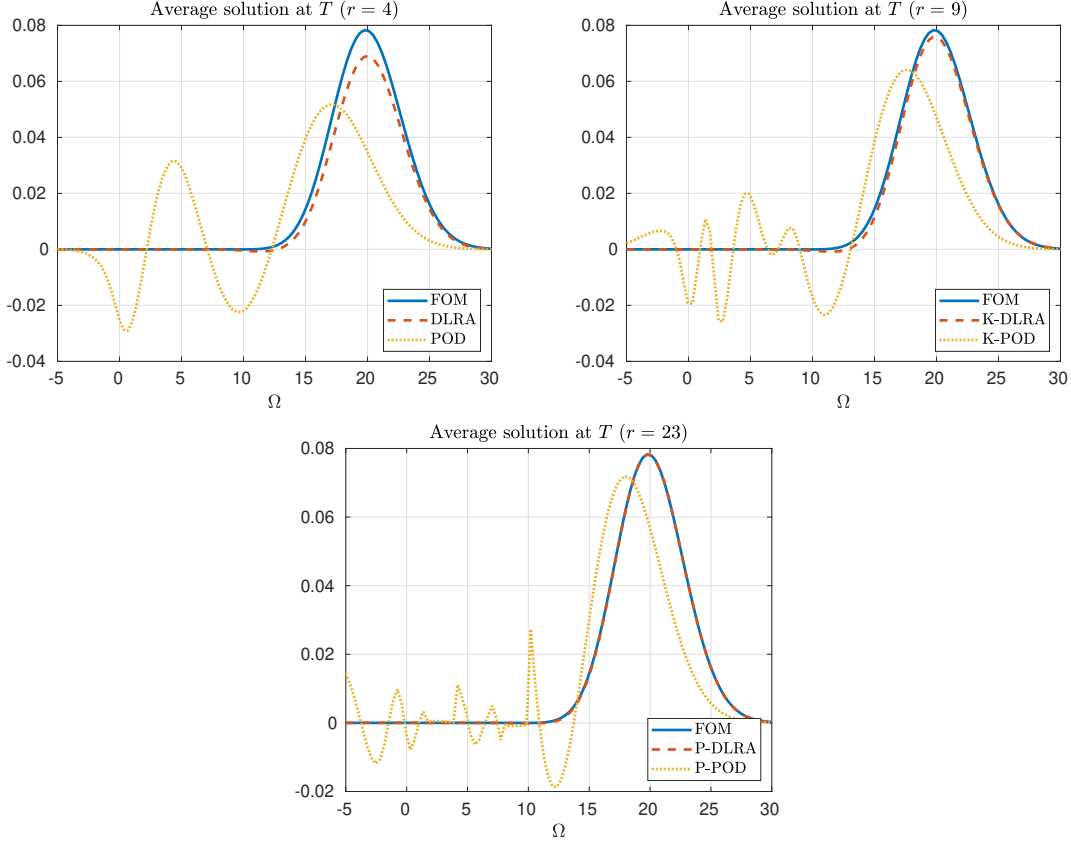


FIGURE 2. Experiment 2. Solutions averaged in \mathcal{P}_h at the final time T . *Top*: FOM, DLRA, and POD for $r = 4$. *Bottom left*: FOM, K-DLRA, and K-POD for $r = 9$ ($r_2 = 5$). *Bottom right*: FOM, P-DLRA, and P-POD for $r = 23$ ($r_2 = 19$).

For the sake of completeness, Figure 4 presents the evolution of the control error $E_c(t)$. In the left panel, we depict the control error for DLRA, K-DLRA, and P-DLRA, while the right panel presents a similar plot for POD, K-POD, and P-POD. Initially, DLRA and K-DLRA show similar performance to POD and K-POD at the beginning of the simulation. However, after $t = 0.7$, the control error for DLRA and K-DLRA decreases significantly, outperforming the performance of POD and K-POD. A similar trend is observed for P-DLRA: although P-POD initially benefits from the Riccati information, by $t = 0.65$, P-DLRA becomes more accurate than P-POD. On average, in terms of control accuracy, POD and K-POD perform similarly to DLRA and K-DLRA. P-POD. However, P-POD performs better than P-DLRA in terms of control accuracy, on average. Nonetheless, it is important to note that POD, K-POD, and even P-POD fail to adequately represent the dynamics, as shown in Figure 2, leading to a degradation in control accuracy in time.

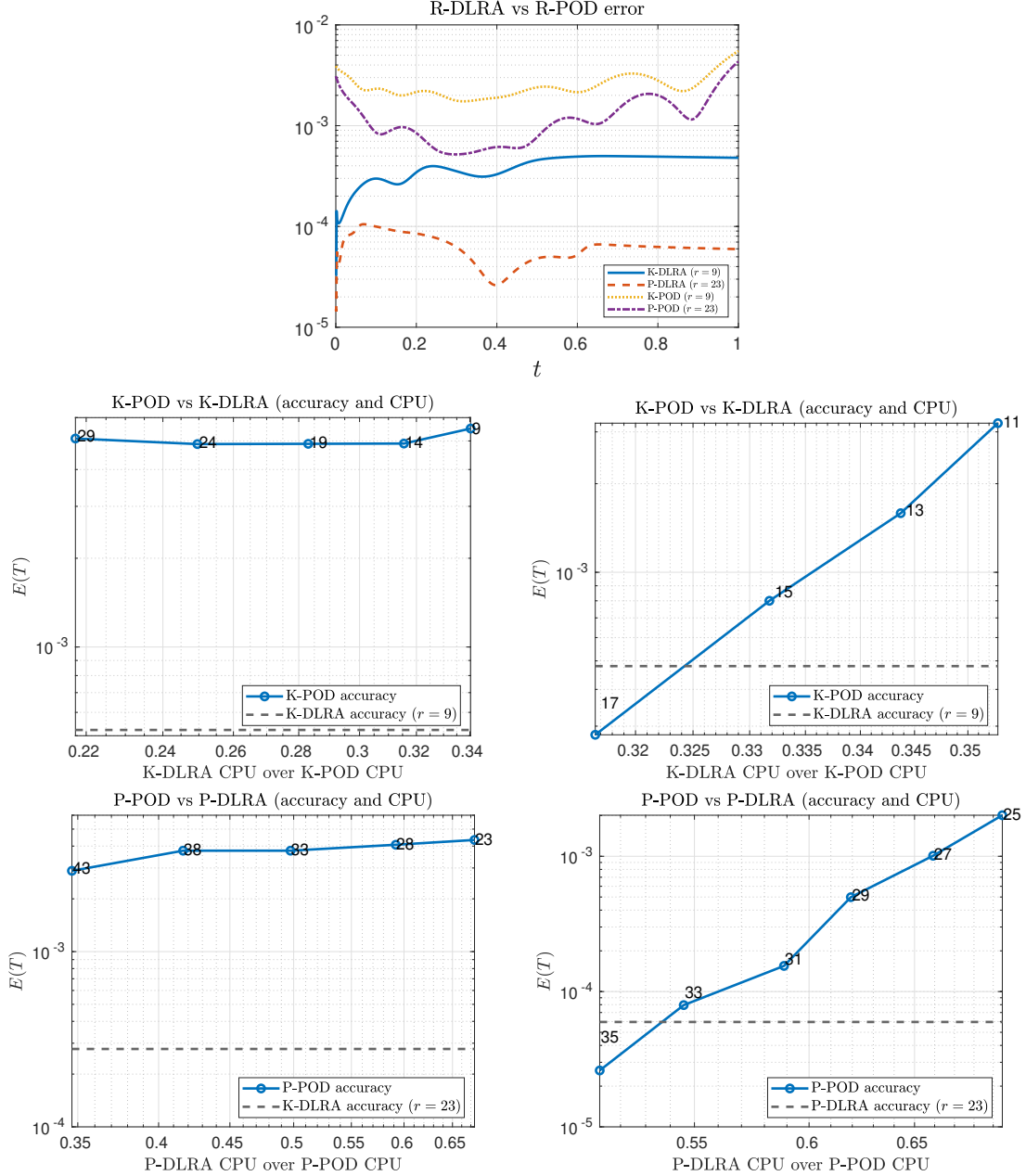


FIGURE 3. Experiment 2. *Top*: Evolution of $E(t)$ for K-POD, K-DLRA, P-POD, and P-DLRA with $r = 9$ and $r = 23$, respectively. *Middle left*: K-POD final accuracy with CPU times for increasing values of r_2 to be compared to the final accuracy of the K-DLRA. *Bottom left*: analogous representation for P-POD. *Middle right*: K-POD final accuracy with CPU times for increasing values of r_1 to be compared to the final accuracy of the K-DLRA. *Bottom right*: analogous representation for P-POD.

Remark 6.1 (The role of the control). *In Figure 4, we notice that the DLRA strategies, at the beginning of the simulation struggle to represent the control action. This might seem unexpected, but we recall that the DLRA process is not an explore-compress algorithm over the controlled trajectory,*

but it only relies on the initial state, with scarce (e.g., *K-DLRA* and *P-DLRA*) or no control information (*DLRA*). In contrast, the *POD* strategies have significantly more information regarding the control action, as the basis functions are constructed using the controlled dynamics. This additional control-related information can aid in more accurately recovering the control action at the beginning of the simulation.

TABLE 2. Experiment 2. CPU comparison for *DLRA*, *POD*, *K-DLRA*, *K-POD*, *P-DLRA* and *P-POD*.

	$r = 4$		$r = 9$		$r = 23$	
	<i>DLRA</i>	<i>POD</i>	<i>K-DLRA</i>	<i>K-POD</i>	<i>P-DLRA</i>	<i>P-POD</i>
global CPU	122	496	173	509	458	680
speedup	71	17	50	17	19	12

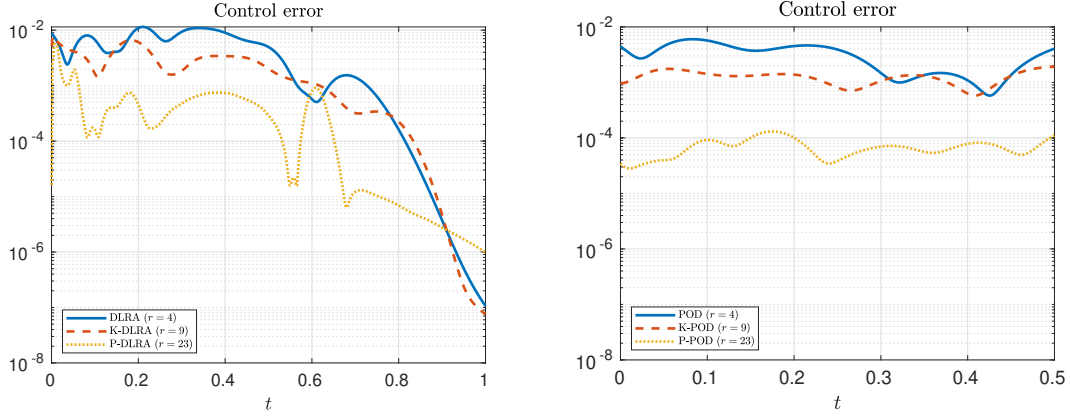


FIGURE 4. Experiment 2. Evolution of $E_c(t)$. *Left plot*: *DLRA*, *K-DLRA*, and *P-DLRA*. *Right plot*: analogous plot for *POD*, *K-POD*, and *P-POD*.

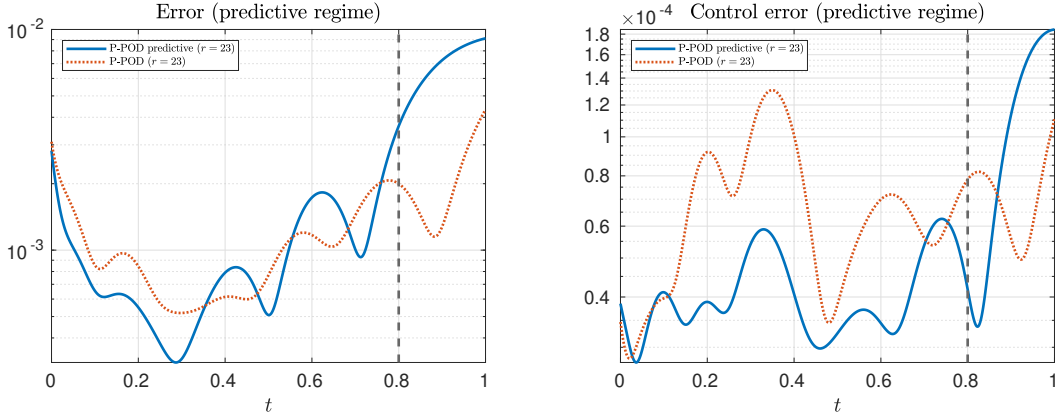


FIGURE 5. Experiment 2, predictive regime for *P-POD*. *Left plot*: evolution of $E(t)$ for *P-POD* in the predictive regime and *P-POD*. *Right plot*: analogous plot for $E_c(t)$.

Remark 6.2 (The actual advantage of DLRA). *Thus far, we have focused on the reconstructive regime of POD. However, it is important to emphasize that DLRA and its Riccati-based variants operate as on-the-fly processes, eliminating the need for a training phase. This represents a significant advantage over POD strategies, which may fail in a predictive setting. For completeness, we conduct a simulation using P-POD (the most effective POD-based reduction method), where the snapshots are taken from the same dynamics as the previous test case but limited to $t = 0.8$, with the number of snapshots fixed at $N_s = 1600$. As expected, the accuracy of P-POD significantly deteriorates towards the end of the simulation, where no prior information is available. Indeed, from the left plot of Figure 5 we observe that in the predictive regime, P-POD performs worse than its reconstructive counterpart. By comparison with Figure 3, we can also notice that the error for the P-DLRA does not increase in time. This behavior is unsurprising, given that DLRA does not rely on training or require prior system information. The same conclusions are drawn from the right plot of Figure 5, which depicts the control error for P-POD in both the predictive and reconstructive regimes. Once again, we note that by the end of the simulation, P-DLRA outperforms P-POD in representing the control even in the reconstructive regime, see Figure 4. For these reasons, in the next test, we only focus on the reconstructive regime, the only setting where the POD strategies might be competitive compared to the DLRA approaches.*

6.2. 2D Burgers' equation. We define the computational domain $\Omega = [-10, 10] \times [-10, 10]$ and the time interval $I = [0, T]$, with $T = 0.5$. The optimal control problem we solve is:

$$(6.3) \quad J(u, y_0) = \int_0^{+\infty} \int_{\omega_o} |y(t, x)|^2 dx + 0.1 \int_{\omega_c} |u(t, x)|^2 dx dt,$$

subject to

$$(6.4) \quad \frac{d}{dt}y(t, x) + y(t, x)\nabla \cdot y(t, x) + 20\nabla \cdot y(t, x) = u(t, x)\chi_{\omega_c}(x),$$

where $\omega_c = [-5, 0] \times [-5, 0]$ is the control domain, $\omega_o = [0, 5] \times [0, 5]$ is the observation domain, and $x = (x_1, x_2)$ is the spatial variable. The parametric initial condition is $y_0(x; \mu) = \mu_1 e^{-\mu_2[(x_1+2)^2+(x_2+2)^2]}$ for $\mu = (\mu_1, \mu_2) \in \mathcal{P} = [0.01, 0.05] \times [0.1, 0.3]$. Homogeneous Neumann boundary conditions are imposed for the boundary $\partial\Omega$. For the space discretization, we apply a Finite Difference scheme. The dimension of the FOM is $N_h = 200$. In time, we perform a midpoint integration scheme with $\Delta t = 10^{-3}$. As in the previous case, the POD and R-POD models are built with a 4×4 parametric grid over \mathcal{P} , with 100 snapshots in time for each parameter, resulting in a total of $N_s = 1600$ snapshots. The DLRA and R-DLRA approaches compute the solution at all time instances using a 20×20 parametric grid over \mathcal{P} , corresponding to $p = 400$ parameters. This set of parameters is the testing parametric set for the POD methods. The order of the parameters for the C-NK strategy follows the one proposed in Section 6.1. The performances are tested in terms of CPU times, $E(t)$ and $E_c(t)$. The basis functions for DLRA and R-DLRA have been selected using the same energy criterion as in Experiment 1 and Experiment 2. The criterion leads to $r = 3$ for DLRA and $r = r_1 + r_2 = 11$ and $r = r_1 + r_2 = 41$, with $r_1 = 3$ and $r_2 = 9$ and $r_2 = 38$, for K-DLRA and P-DLRA, respectively. We recall that r_1 is the number of basis from the SVD of the initial state, while r_2 is the number of basis functions related to the additional Riccati information, computed in the same parametric set of the standard DLRA approach.

We start with a qualitative analysis in Figure 6, where we plot the averaged solution in \mathcal{P}_h at the final time. As in the one-dimensional case, DLRA and K-DLRA present an agreement with the FOM solution, but the accuracy is highly increased when the P-DLRA is used. All the POD strategies fail to represent the FOM solution, with many spurious oscillations. From a quantitative viewpoint, in the left plot of Figure 7, we show the evolution of E in time for DLRA and POD. As expected, DLRA outperforms POD. On the right plot, we fix the DLRA final accuracy $E(T)$ for $r = 3$ and we plot the final accuracy of the POD increasing the number of basis functions. To achieve comparable accuracy to DLRA, POD requires $r = 12$ basis functions. Nonetheless, DLRA is unparalleled in terms of computational efficiency, being nearly two orders of magnitude faster. The CPU times and the corresponding speedups relative to the FOM solution are reported in the first

column of Table 3, where it is evident that the DLRA approach significantly outperforms the POD approach in terms of speed.

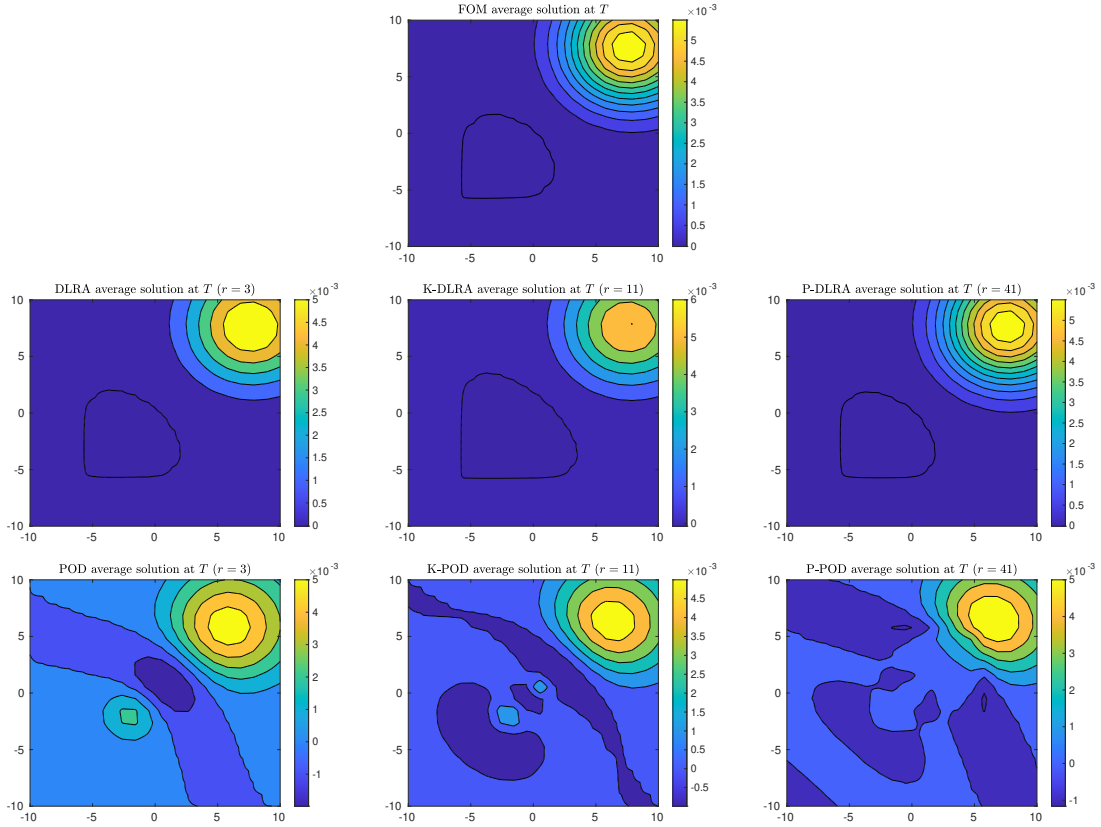


FIGURE 6. Experiment 3. Solutions averaged in \mathcal{P}_h at the final time T . *Top*: FOM. *Middle row*: DLRA ($r = 3$), K-DLRA ($r = 11$), and P-DLRA ($r = 41$). *Bottom row*: POD ($r = 3$), K-POD ($r = 11$), and P-POD ($r = 41$)

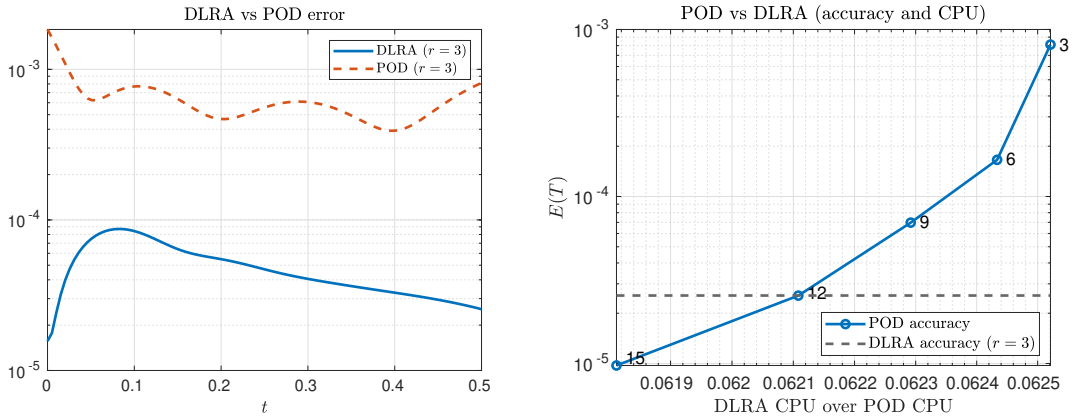


FIGURE 7. Experiment 3. *Left*: Evolution of $E(t)$ for DLRA and POD for $r = 3$. *Right*: POD final accuracy plot with CPU times for increasing values of r to be compared to the final accuracy of the DLRA approach.

The same analysis is performed in Figure 8 for the R-DLRA and R-POD approaches. Firstly, the top plot demonstrates that K-DLRA offers a slight improvement over DLRA, as observed when compared to Figure 7.

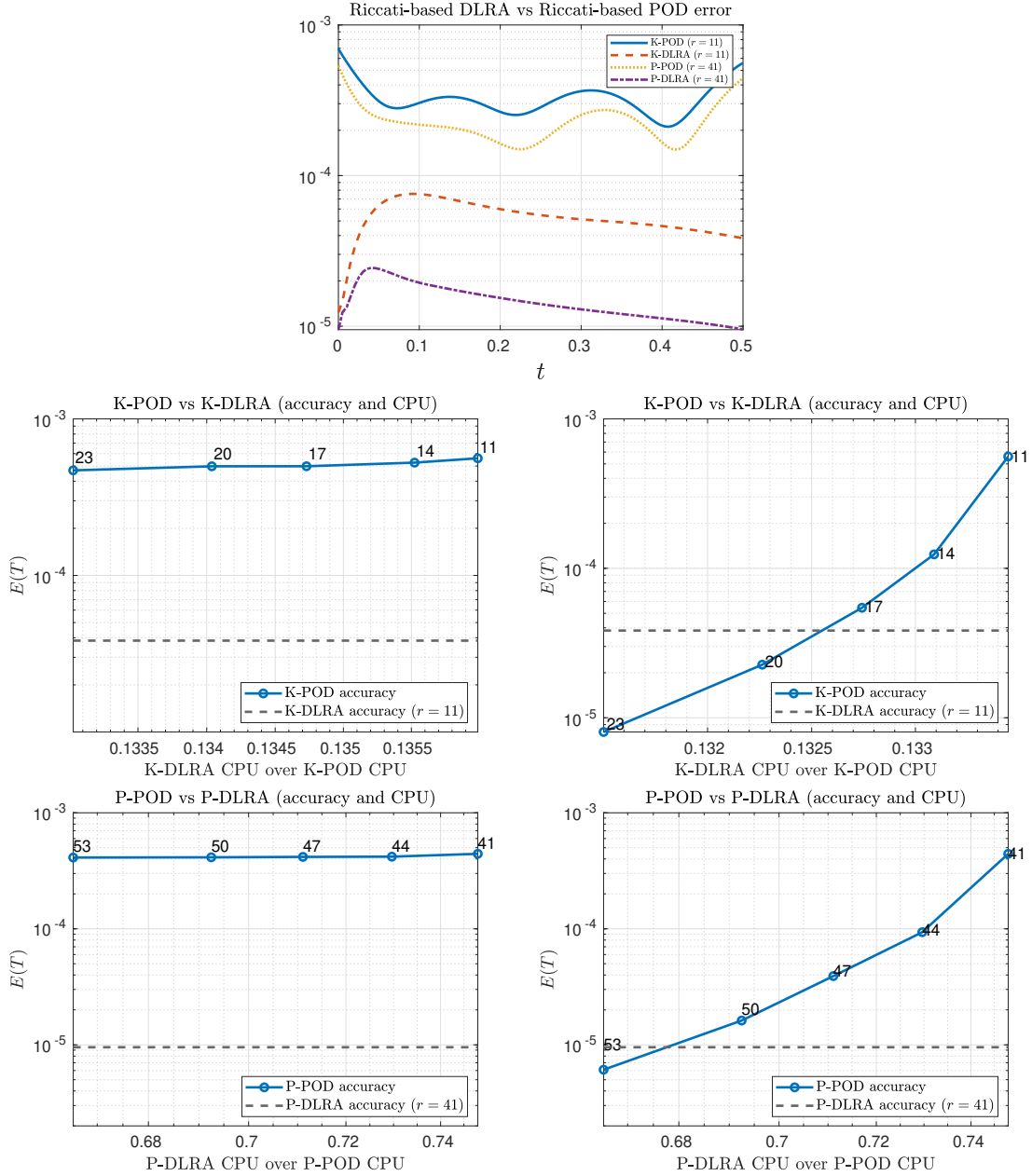


FIGURE 8. Experiment 3. *Top*: Evolution of $E(t)$ for K-POD, K-DLRA, P-POD, and P-DLRA with $r = 11$ and $r = 41$, respectively. *Middle left*: K-POD final accuracy with CPU times for increasing values of r_2 to be compared to the final accuracy of the K-DLRA. *Bottom left*: analogous representation for P-POD. *Middle right*: K-POD final accuracy with CPU times for increasing values of r_1 to be compared to the final accuracy of the K-DLRA. *Bottom right*: analogous representation for P-POD.

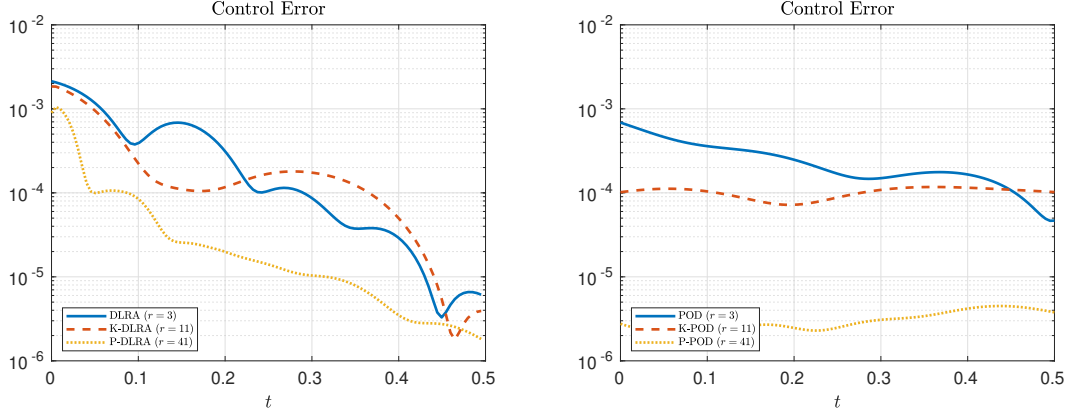


FIGURE 9. Experiment 3. Evolution of $E_c(t)$. *Left plot*: DLRA, K-DLRA, and P-DLRA. *Right*: analogous plot for POD, K-POD, and P-POD.

The middle plots present a performance analysis of the final accuracy and CPU times for K-POD, compared with the accuracy and CPU times of K-DLRA for $r = 11$. Similarly to the previous test case, larger values of r_2 do not increase the K-POD accuracy. The only effective way to improve the accuracy is by increasing r_1 . Notably, K-POD requires approximately twenty basis functions to be competitive with K-DLRA. However, K-DLRA remains nearly ten times faster in terms of CPU time. In the bottom plots, a similar analysis is conducted for P-POD. Increasing r_2 proves ineffective, while fixing $r_2 = 38$ and setting $r_1 = 15$ let the P-POD achieve an accuracy comparable to P-DLRA, which still outperforms the POD counterpart in terms of computational speed. Table 3 summarizes all the CPU times for all the strategies considered. For completeness, Figure 9 illustrates the evolution of $E_c(t)$. On the left, we depict it for DLRA, K-DLRA, and P-DLRA. The same plot is proposed on the right for POD, K-POD, and P-POD. As in the one-dimensional case, DLRA and K-DLRA are comparable to POD and K-POD at the beginning of the simulation. The DLRA and the K-DLRA control errors drastically decrease after $t = 0.3$ and start to outperform the POD and the K-POD. However, for this test case, P-POD is very accurate in terms of control error. By the end of the simulation, P-DLRA reaches the same order of accuracy. It is important to note that while P-POD is accurate for control errors, it remains less effective in recovering the dynamics, as shown in Figure 6. Concluding, the DLRA-based approaches outperform the corresponding POD versions for all the metrics taken into consideration for the state dynamics. The P-DLRA strategy is the most accurate approach; however, as expected, it requires a greater computational time due to the large number of basis functions needed for the simulation.

TABLE 3. Experiment 3. CPU comparison for DLRA, POD, K-DLRA, K-POD, P-DLRA and P-POD.

	$r = 3$		$r = 11$		$r = 41$	
	DLRA	POD	K-DLRA	K-POD	P-DLRA	P-POD
global CPU	169	$2.71 \cdot 10^3$	370	$2.78 \cdot 10^3$	$3.31 \cdot 10^3$	$4.42 \cdot 10^3$
speedup	374	23	170	22	19	14

7. CONCLUSIONS

This contribution introduces DLRA-based approaches to address parametric nonlinear feedback control under transport phenomena for stabilizing dynamical systems within the infinite horizon optimal control framework. To the best of the authors' knowledge, this is the first study to explore this direction. The DLRA framework has been enhanced through two key strategies: (i) the C-NK method, which accelerates the convergence of the iterative solution of the SDREs, and (ii) the

leveraging of the Riccati information, leading to the development of two novel algorithms, K-DLRA and P-DLRA, that improve the accuracy of standard DLRA in control problems. These algorithms have been benchmarked against their POD counterparts in terms of accuracy with respect to the FOM solution and computational efficiency. The DLRA approaches have demonstrated superior performance in accelerating the solution of controlled dynamical systems than the FOM and the POD.

The results have been validated through one- and two-dimensional test cases involving infinite horizon feedback control for Burgers' equations. Notably, the C-NK strategy has been theoretically substantiated via a rigorous sensitivity analysis of the initial guesses for the NK iterative solver.

This research opens several promising investigations for future work. Numerical results indicate that DLRA has challenges in recovering the FOM control, as highlighted in Remark 6.1. Potential future development is to combine the strengths of POD-based methods to recover control with the high precision of DLRA-based methods in the state dynamic, with the final goal of proposing an efficient algorithm with increased accuracy in representing control actions. Another promising improvement involves introducing adaptivity in the number of basis functions over time. Moreover, we believe that DLRA and R-DLRA might be of indisputable utility in more complicated applications in real-life scenarios, most of all in transient and convection-dominated settings.

ACKNOWLEDGMENTS

We acknowledge the INdAM - GNCS Project “Metodi di riduzione di modello ed approssimazioni di rango basso per problemi alto-dimensionali” (CUP_E53C23001670001).

MS thanks the “20227K44ME - Full and Reduced order modelling of coupled systems: focus on non-matching methods and automatic learning (FaReX)” project – funded by European Union – Next Generation EU within the PRIN 2022 program (D.D. 104 - 02/02/2022 Ministero dell'Università e della Ricerca). This manuscript reflects only the authors' views and opinions and the Ministry cannot be considered responsible for them. The work of MS has been supported by European Union's Horizon 2020 research and innovation programme under the Marie Skłodowska-Curie Actions, grant agreement 872442 (ARIA). MS thanks the ECCOMAS EYIC Grant “CRAFT: Control and Reg-reduction in Applications for Flow Turbulence”.

The authors express their sincere gratitude for the many insightful discussions with Stefano Massei and Cecilia Pagliantini.

REFERENCES

- [1] A. Alla, B. Haasdonk, and A. Schmidt. Feedback control of parametrized PDEs via model order reduction and dynamic programming principle. *Advances in Computational Mathematics*, 46(1):9, 2020. doi:10.1007/s10444-020-09744-8.
- [2] H. T. Banks, B. M. Lewis, and H. T. Tran. Nonlinear feedback controllers and compensators: a state-dependent Riccati equation approach. *Computational Optimization and Applications*, 37(2):177–218, 2007. doi:10.1007/s10589-007-9015-2.
- [3] R. H. Bartels and G. W. Stewart. Algorithm 432 [C2]: solution of the matrix equation $AX + XB = C$ [F4]. *Communications of the ACM*, 15(9):820–826, 1972. doi:10.1145/361573.361582.
- [4] P. Benner, Z. Bujanović, P. Kürschner, and J. Saak. A numerical comparison of different solvers for Large-Scale, Continuous-Time Algebraic Riccati Equations and LQR problems. *SIAM Journal on Scientific Computing*, 42(2):A957–A996, 2020. doi:10.1137/18m1220960.
- [5] E. Celledoni and B. Owren. A class of intrinsic schemes for orthogonal integration. *SIAM Journal on Numerical Analysis*, 40(6):2069–2084, 2002. doi:10.1137/S0036142901385143.
- [6] T. Çimen. State-dependent Riccati equation (SDRE) control: a survey. *IFAC Proceedings Volumes*, 41(2):3761–3775, 2008. doi:10.3182/20080706-5-KR-1001.00635.
- [7] J. Darbon, G. P. Langlois, and T. Meng. Overcoming the curse of dimensionality for some Hamilton–Jacobi partial differential equations via neural network architectures. *Research in the Mathematical Sciences*, 7(3), 2020. doi:10.1007/s40687-020-00215-6.
- [8] J. de Frutos, B. Garcia-Archilla, and J. Novo. Optimal bounds for POD approximations of infinite horizon control problems based on time derivatives. 2023. arXiv:2310.10552.
- [9] R. A. DeVore. *Chapter 3: The Theoretical Foundation of Reduced Basis Methods*, pages 137–168. doi:10.1137/1.9781611974829.ch3.

- [10] S. Dolgov, D. Kalise, and L. Saluzzi. Data-driven tensor train gradient cross approximation for Hamilton–Jacobi–Bellman equations. *SIAM Journal on Scientific Computing*, 45(5):A2153–A2184, 2023. doi:10.1137/22M1498401.
- [11] S. Dolgov, D. Kalise, and L. Saluzzi. Statistical proper orthogonal decomposition for model reduction in feedback control, 2023. URL: <https://arxiv.org/abs/2311.16332>, arXiv:2311.16332.
- [12] M. Eigel, R. Schneider, and D. Sommer. Dynamical low-rank approximations of solutions to the Hamilton–Jacobi–Bellman equation. *Numerical Linear Algebra with Applications*, 30(3):e2463, 2023. doi:10.1002/nla.2463.
- [13] M. Falcone, G. Kirsten, and L. Saluzzi. Approximation of Optimal Control Problems for the Navier–Stokes equation via multilinear HJB-POD. *Applied Mathematics and Computation*, 442:127722, 2023. doi:10.1016/j.amc.2022.127722.
- [14] P. Gahinet and A. Laub. Computable bounds for the sensitivity of the algebraic riccati equation. *SIAM journal on control and optimization*, 28(6):1461–1480, 1990. doi:10.1137/0328077.
- [15] J. Garcke and A. Kröner. Suboptimal feedback control of PDEs by solving HJB equations on adaptive sparse grids. *Journal of Scientific Computing*, 70(1):1–28, 2016. doi:10.1007/s10915-016-0240-7.
- [16] E. Hairer, C. Lubich, and G. Wanner. *Geometric Numerical Integration. Second*. Springer Series in Computational Mathematics, vol. 31. Springer, Berlin, 2006.
- [17] M. Hinze and S. Volkwein. Proper orthogonal decomposition surrogate models for nonlinear dynamical systems: Error estimates and suboptimal control. In *Dimension Reduction of Large-Scale Systems: Proceedings of a Workshop held in Oberwolfach, Germany, October 19–25, 2003*, pages 261–306. Springer, 2005.
- [18] M. Hinze and S. Volkwein. Proper orthogonal decomposition surrogate models for nonlinear dynamical systems: Error estimates and suboptimal control. In *Dimension reduction of large-scale systems*, pages 261–306. Springer, 2005.
- [19] H. Keller. *Lectures on Numerical Methods in Bifurcation Problems*. 1988.
- [20] C. Kenney and G. Hewer. The sensitivity of the algebraic and differential Riccati equations. *SIAM journal on control and optimization*, 28(1):50–69, 1990. doi:doi.org/10.1137/0328003.
- [21] G. Kirsten and L. Saluzzi. A Multilinear HJB-POD Method for the Optimal Control of PDEs on a Tree Structure. *Journal of Scientific Computing*, 101(2):41, 2024. doi:10.1007/s10915-024-02683-2.
- [22] G. Kirsten and V. Simoncini. Order reduction methods for solving Large-Scale Differential Matrix Riccati Equations. *SIAM Journal on Scientific Computing*, 42(4):A2182–A2205, 2020. doi:10.1137/19m1264217.
- [23] D. Kleinman. On an iterative technique for Riccati equation computations. *IEEE Transactions on Automatic Control*, 13(1):114–115, 1968. doi:10.1109/TAC.1968.1098829.
- [24] O. Koch and C. Lubich. Dynamical low-rank approximation. *SIAM Journal on Matrix Analysis and Applications*, 29(2):434–454, 2007. doi:10.1137/050639703.
- [25] K. Kunisch and S. Volkwein. Control of the Burgers equation by a reduced-order approach using proper orthogonal decomposition. *Journal of Optimization Theory and Applications*, 102(2):345 – 371, 1999. doi:10.1023/A:1021732508059.
- [26] K. Kunisch, S. Volkwein, and L. Xie. HJB-POD based feedback design for the optimal control of evolution problems. *SIAM J. on Applied Dynamical Systems*, 4:701–722, 2004. doi:10.1137/030600485.
- [27] K. Kunisch and D. Walter. Semiglobal optimal feedback stabilization of autonomous systems via deep neural network approximation. *ESAIM: Control, Optimisation and Calculus of Variations*, 27:16, 2021. doi:10.1051/cocv/2021009.
- [28] P. Lancaster. *Algebraic Riccati Equations*. Oxford Science Publications/The Clarendon Press, Oxford University Press, 1995.
- [29] M. Oster, L. Sallandt, and R. Schneider. Approximating optimal feedback controllers of finite horizon control problems using hierarchical tensor formats. *SIAM Journal on Scientific Computing*, 44(3):B746–B770, 2022.
- [30] C. Pagliantini. Dynamical reduced basis methods for hamiltonian systems. *Numerische Mathematik*, 2021. doi:10.1007/s00211-021-01211-w.
- [31] B. Peherstorfer. Model Reduction for Transport-Dominated Problems via Online Adaptive Bases and Adaptive Sampling. *SIAM Journal on Scientific Computing*, 42(5):A2803–A2836, 2020. doi:10.1137/19M1257275.
- [32] F. Pichi, M. Strazzullo, F. Ballarin, and G. Rozza. Driving bifurcating parametrized nonlinear PDEs by optimal control strategies: Application to Navier–Stokes equations with model order reduction. *ESAIM: Mathematical Modelling and Numerical Analysis*, 56(4):1361 – 1400, 2022. doi:10.1051/m2an/2022044.
- [33] A. Quarteroni, A. Manzoni, and F. Negri. *Reduced Basis Methods for Partial Differential Equations: An Introduction*. La Matematica per Il 3+2, 92. Springer International Publishing, Cham, 1st ed. 2016. edition, 2016. doi:10.1007/978-3-319-15431-2.
- [34] T. P. Sapsis and P. F. Lermusiaux. Dynamically orthogonal field equations for continuous stochastic dynamical systems. *Physica D: Nonlinear Phenomena*, 238(23-24):2347–2360, 2009. doi:10.1016/j.physd.2009.09.017.
- [35] A. Schmidt, M. Dihlmann, and B. Haasdonk. Basis generation approaches for a reduced basis linear quadratic regulator. *IFAC-PapersOnLine*, 48(1):713–718, 2015.
- [36] A. Schmidt and B. Haasdonk. Reduced basis approximation of large scale parametric algebraic Riccati equations. *ESAIM: Control, Optimisation and Calculus of Variations*, 24(1):129–151, 2018. doi:10.1051/cocv/2017011.
- [37] G. Söderlind. The logarithmic norm. History and modern theory. *BIT Numerical Mathematics*, 46:631–652, 2006. doi:10.1007/s10543-006-0069-9.

- [38] M. Strazzullo, F. Ballarin, and G. Rozza. POD-Galerkin model order reduction for parametrized nonlinear time dependent optimal flow control: an application to Shallow Water Equations. *Journal of Numerical Mathematics*, 30(1):63–84, 2022. doi:10.1515/jnma-2020-0098.
- [39] M. Strazzullo and F. Vicini. POD-Based reduced order methods for optimal control problems governed by parametric partial differential equation with varying boundary control. *Applied Mathematics and Computation*, 457, 2023. doi:10.1016/j.amc.2023.128191.
- [40] M. Zhou, J. Han, and J. Lu. Actor-Critic Method for High Dimensional Static Hamilton–Jacobi–Bellman Partial Differential Equations based on Neural Networks. *SIAM Journal on Scientific Computing*, 43(6):A4043–A4066, 2021. doi:10.1137/21m1402303.

APPENDIX A. ADDITIONAL RESULTS ON THE SENSITIVITY ESTIMATES

In this Appendix, we collect all the results needed to prove and validate the estimate of Section 3. Section A.1 details the propositions necessary to the proofs of Theorems 2.4 and 3.3. In Section A.2, we propose a numerical example validating the theoretical sensitivity analysis.

A.1. Auxiliary results.

Proposition A.1. *Given a vector field $f(t, y)$ satisfying the one-sided Lipschitz condition (3.2), then the following estimate holds*

$$(A.1) \quad \|y(t; y_0) - y(t; \tilde{y}_0)\| \leq \|y_0 - \tilde{y}_0\| e^{Lt}.$$

Proof. Let us denote by $y_1(t)$ and $y_2(t)$ the solutions of the ODE with corresponding initial condition y_0 and \tilde{y}_0 and define $\Delta y(t) = y_1(t) - y_2(t)$. Then we have:

$$\Delta y(t) \cdot \frac{d}{dt} \Delta y(t) = \Delta y(t) \cdot (f(t, y_1(t)) - f(t, y_2(t))).$$

Using the one-sided Lipschitz condition:

$$\Delta y(t) \cdot (f(t, y_1(t)) - f(t, y_2(t))) \leq L \|\Delta y(t)\|^2.$$

Since $\frac{d}{dt} \|\Delta y(t)\|^2 = 2\Delta y(t) \cdot \frac{d}{dt} \Delta y(t)$, we have:

$$\frac{d}{dt} \|\Delta y(t)\|^2 \leq 2L \|\Delta y(t)\|^2.$$

By Gronwall’s inequality, we obtain the result. \square

Proposition A.2. *Given the assumptions (1)-(2), the vector field $f(t, y) = A_{cl}(y)y$ satisfies the one-sided Lipschitz condition (3.2) in a domain Ω with constant*

$$L = \max_{x \in \Omega} \log m(A_{cl}(x)) + L_{cl} \max_{y \in \Omega} \|y\|.$$

Proof. We aim to verify if the function $A_{cl}(y)y$ satisfies condition (3.2). Let us manipulate the left-hand side of condition (3.2) to obtain

$$(x - y)^\top (A_{cl}(x)x - A_{cl}(y)y) = (x - y)^\top A_{cl}(x)(x - y) + (x - y)^\top (A_{cl}(x) - A_{cl}(y))y$$

By the definition of logarithmic norm we obtain

$$(x - y)^\top A_{cl}(x)(x - y) \leq \log m(A_{cl}(x)) \|x - y\|^2$$

while by assumption (1)

$$|(x - y)^\top (A_{cl}(x) - A_{cl}(y))y| \leq L_{cl} \|y\| \|x - y\|^2$$

Considering the maximum in x and y over the domain Ω gives the result. \square

Corollary A.3. *Given the assumptions (1)-(4), the following estimate holds*

$$\|y(t; y_0(\mu)) - y(t; y_0(\tilde{\mu}))\| \leq L_{y_0} \|\mu - \tilde{\mu}\| e^{Lt},$$

with $L = \max_{x \in \Omega} \log m(A_{cl}(x)) + L_{cl} \max_{y \in \Omega} \|y\|$.

Proof. By Proposition A.2, we know that the function $f(t, y) = A_{cl}(y)y$ satisfies the one-sided Lipschitz condition (3.2). Applying Proposition A.1 and assumption (4) we obtain the result. \square

Proposition A.4. *Given $(\nabla A_{cl}(y))y = \left(\left[\frac{\partial}{\partial y_1} A_{cl}(y) \right] y \dots \left[\frac{\partial}{\partial y_d} A_{cl}(y) \right] y \right) \in \mathbb{R}^{d \times d}$ for $y \in \mathbb{R}^d$, if*

$$(A.2) \quad \log m(A_{cl}(y)) + \log m((\nabla A_{cl}(y))y) < 0,$$

then $\|A_{cl}(y(t))y(t)\|$ is decreasing in time.

Proof. Denoting $z(t) = A_{cl}(y(t))y(t)$, we have

$$\begin{aligned} \frac{d}{dt} \|z(t)\|^2 &= 2z(t)^\top [(\nabla A_{cl}(y(t)))y(t) + A(y(t))] z(t) \leq \\ &2(\log m(A(y)) + \log m((\nabla A_{cl}(y))y)) \|z(t)\|^2 \end{aligned}$$

and the result comes from assumption (A.2). \square

A.2. A Numerical validation. In this section, we want to show how the theoretical findings derived in Section 3 can be applied in practice. Let us consider the optimal control problem driven by the following nonlinear reaction-diffusion equation:

$$(A.3) \quad \frac{d}{dt} y(t, x) = \sigma \partial_{xx} y(t, x) + y(t, x)^2 + u(t, x), \quad (t, x) \in \mathbb{R}^+ \times [0, 2],$$

with associated cost functional

$$J(u, y_0) = \int_0^{+\infty} \int_{\Omega} |y(t, x)|^2 dx + \int_{\Omega} |u(t, x)|^2 dx dt.$$

Fixing $\sigma = 10^{-3}$ and performing a semidiscretization via finite difference with $N_h = 50$ grid points, we obtain

$$\dot{y}(t) = A(y)y(t) + u(t),$$

where

$$A(y) = \sigma A_0 + \text{diag}(y \circ y),$$

with A_0 arising from the discretization of the Laplacian with Neumann boundary conditions, \circ stands for the Hadamard product and $\text{diag}(v)$ indicates a diagonal matrix with the components of the vector v on the main diagonal.

Let us consider a set of parameterized initial conditions

$$y_0(x; \mu) = \mu \sin(\pi x), \quad \mu \in [1, 10].$$

We note that in this case $A(y)$ is symmetric for all $y \in \mathbb{R}^d$ and the term F is an identity matrix multiplied by a scalar depending on the space discretization. As a result, the closed-loop matrix is symmetric, and all of its eigenvalues are real. Let us denote by $\lambda_{\mu_1, \mu_2, t_1, t_2}$ the maximum eigenvalue of the matrix $A_{\mu_2, t_2} - F P_{\mu_1, t_1}$, i.e., the starting closed-loop matrix for the parameter μ_2 at time t_2 using as initial guess P_{μ_1, t_1} . Our aim is to verify whenever this value is negative and, hence, P_{μ_1, t_1} represents a stabilizing initial guess. We proceed applying the following steps:

- (1) we start at initial time from $\mu_1 = 1$ and we solve the following SDRE

$$A_{\mu_1, 0}^\top P_{\mu_1, 0} + P_{\mu_1, 0} A_{\mu_1, 0} - P_{\mu_1, 0} F P_{\mu_1, 0} = -Q,$$

using the Matlab function `icare`;

- (2) we compute the approximate solution $H_{\mu_1, 0}$ of the Lyapunov equation (3.8) by the Matlab function `lyap`;
- (3) we note that

$$\|\Delta A_{\mu_1, \mu_2, 0, 0}\|^2 = |\mu_1^2 - \mu_2^2| \|\text{diag}(\sin(\pi x))\|^2,$$

where $\sin(\pi x) = [\sin(\pi x_1), \dots, \sin(\pi x_d)]^\top$;

(4) condition (3.7) now reads

$$|\mu_1^2 - \mu_2^2| \leq c = \frac{1}{4\|H_{\mu_1,0}\|^2\|diag(\sin(\pi x))\|^2},$$

where the right-hand side is equal to 1.0011 in this case. Hence, condition (3.7) is satisfied if

$$\Delta\mu \leq -1 + \sqrt{1+c} \approx 0.4146.$$

If we consider $\Delta\mu = 0.45$, the condition (3.7) is not satisfied and we note that the maximum eigenvalue of the closed loop matrix $A_{\mu_2,0} - FP_{\mu_1,0}$ is positive ($\lambda_{\mu_1,\mu_2,0,0} = 0.0019$), hence $P_{\mu_1,0}$ is not a stabilizing initial guess. On the other hand, considering $\Delta\mu = 0.4$, as expected, $P_{\mu_1,0}$ is a stabilizing initial guess ($\lambda_{\mu_1,\mu_2,0,0} = -0.1342$). This provides a strategy to compute the parameter stepsize to ensure the cascade approach at the initial time.

Now let us consider the time integration with final time $T = 0.1$ with $\Delta\mu = 0.1$. In the top-left panel of Figure 10, we compare the behavior in time of the terms $g_1(t) = \|\Delta A_{\mu,\tilde{\mu},t,t}\|$ (denoted in the plot as Lower Estimate), $g_2(t) = L_A L_{y_0} \|\mu - \tilde{\mu}\| e^{Lt}$ (One-sided Upper Estimate) and $g_3(t) = \frac{1}{2\|H_{\mu,t}\|}$ (Upper Estimate). The constants L and L_A can be estimated along the trajectories in the following way

$$L_A = \max_i \frac{\|A(y_{\mu_1,t_i}) - A(y_{\mu_2,t_i})\|}{\|y_{\mu_1,t_i} - y_{\mu_2,t_i}\|},$$

$$L = \max_i \frac{(A_{cl}(y_{\mu_1,t_i}) - A_{cl}(y_{\mu_2,t_i}))^\top (y_{\mu_1,t_i} - y_{\mu_2,t_i})}{\|y_{\mu_1,t_i} - y_{\mu_2,t_i}\|}.$$

We note that the upper estimate exhibits an almost constant behavior, remaining close to values around 1.

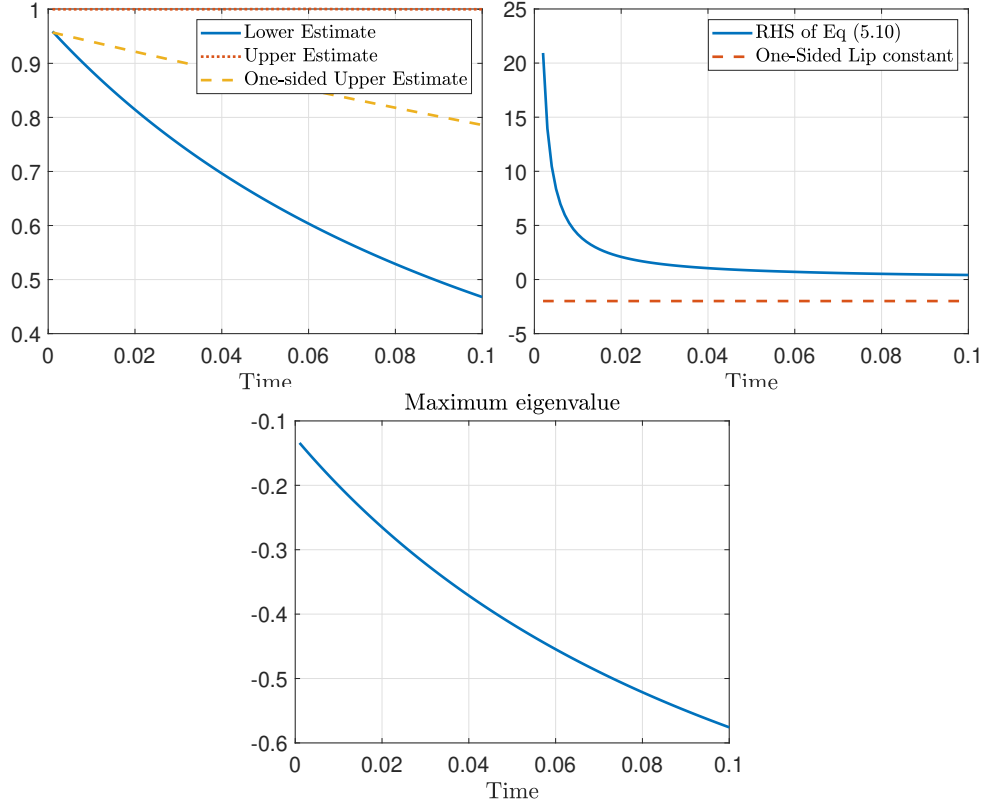


FIGURE 10. *Top*: Verification of the estimate (3.7) (left) and the estimate (3.10) (right). *Bottom*: Maximum eigenvalue $\lambda_{\mu_1,\mu_2,t,t}$ in the time interval $[0, 0.1]$.

On the other hand, the Lower Estimate starts below as expected, since the initial choice for $\Delta\mu$ satisfies the condition (3.7). The estimated one-sided Lipschitz constant L is negative and equal to -1.9897 , reflecting the decreasing behavior of the One-sided Upper Estimate and of the Lower Estimate. Condition (3.10) is depicted in the top-right panel of Figure 10. The right-hand side of the estimate (3.10) is decreasing, but always positive, while the one-sided Lipschitz constant L is negative. Hence, condition (3.10) is satisfied for the entire time interval $[0, 0.1]$. From this, we can infer that $P_{\mu_1, t}$ consistently serves as a stabilizing initial guess. This is demonstrated in the bottom panel of Figure 10, where the maximum eigenvalue remains negative throughout the time interval. Let us now perform a similar analysis for the time step Δt . For simplicity, we will use the explicit Euler method for integration. Given the initial condition $y_{\mu_1, 0} = \sin(\pi x)$, consider the update $y_{\mu_1, \Delta t} = y_{\mu_1, 0} + \Delta t (A(y_{\mu_1, 0}) - FP_{\mu_1, 0}) y_{\mu_1, 0}$. We define $f_{cl, 0}$ as $f_{cl, 0} = (A(y_{\mu_1, 0}) - FP_{\mu_1, 0}) y_{\mu_1, 0}$. Now, we compute:

$$\|\Delta A_{\mu_1, \mu_1, 0, \Delta t}\|^2 = \|\text{diag}(y_{\mu_1, \Delta t} \circ y_{\mu_1, \Delta t}) - \text{diag}(y_{\mu_1, 0} \circ y_{\mu_1, 0})\| = (\Delta t)^2 f_{cl, 0}^2 + 2\Delta t f_{cl, 0} \cdot y_{\mu_1, 0},$$

then condition (3.7) becomes

$$(\Delta t)^2 \|f_{cl, 0}\|^2 + 2\Delta t f_{cl, 0} \cdot y_{\mu_1, 0} - \frac{1}{2\|H_{\mu_1, 0}\|^2} \leq 0,$$

which leads to the solution

$$\Delta t \leq \frac{-f_{cl, 0} \cdot y_{\mu_1, 0} + \sqrt{(f_{cl, 0} \cdot y_{\mu_1, 0})^2 + \frac{1}{2\|H_{\mu_1, 0}\|^2}}}{\|f_{cl, 0}\|^2} \approx 1.5694.$$

In fact, for $\Delta t = 1.6$, the maximum eigenvalue of the closed loop matrix $A(y_{\mu_1, \Delta t}) - FP_{\mu_1, 0}$ is positive ($\lambda_{\mu_1, \mu_1, 0, \Delta t} = 0.8752$), whereas for $\Delta t = 1.5$, it is negative ($\lambda_{\mu_1, \mu_1, 0, \Delta t} = -0.7858$). This section justifies the use of the cascade information in solving the SDRE by means of NK.